DFT-Based Study of the First PCET of the OER on Large (001)-Exposing Anatase TiO_2 Nanoparticles in a Water-Splitting Environment

Patrick Saitta

Submitted in partial fulfillment of the
requirements for the degree of
Doctor of Philosophy
in the Graduate School of Arts and Sciences

COLUMBIA UNIVERSITY

2020

Abstract

DFT-Based Study of the First PCET of the OER on Large (001)-Exposing Anatase TiO_2 Nanoparticles in a Water-Splitting Environment

Patrick Saitta

This dissertation computationally studies the oxygen evolution reaction (OER) that occurs at the surface of titanium dioxide (TiO_2) nanoparticles in water, specifically the first proton-couple electron transfer (PCET) of four sequential PCETs that the overall OER comprises. To do so, we first modelled TiO_2 nanoparticles and developed a realistic passivation scheme for the nanoparticle's surface in an aqueous environment. Additionally, we developed a fragment-based initial guess (FIG) methodology in order to make studying systems approaching real-life nanoparticle sizes computationally tenable. The FIG methodology allowed us to employ hybrid-DFT (B3LYP) calculations to study systems of around 5000 basis functions, or more than 500 atoms. Then, we simulated the PCET by selecting particular points along the PCET reactant pathway and optimizing the system at each of these dozen points. In order to make these optimizations occur in a tractable amount of time, they were run on the STAMPEDE supercomputer operated by the Texas Advanced Computing Center (TACC), implemented with an OpenMP/MPI hybrid parallelization. These optimizations provided us with a picture of the electronic structure changes that occur over the course of the PCET and allowed us to calculate theoretical overpotentials to the PCET, both of which inform our conclusion of the nature of the inefficiency of the solar water-splitting reaction. In short, our studies show the major source of inefficiency to be the thermodynamic instability of the intermediate oxygen species (a hydroxyl

adsorbate) on the surface of the nanoparticle. Additionally, while the hole created by cationization does lower the overpotential of the PCET, we do not find that this is because the two happen concertedly, which would confer stability to the system and lower the total energy, but rather for some other reason. Additionally, we do not find that the hole gets filled by the transferring electron of the PCET, raising questions as to how the OER can continue to occur without the structure of the nanoparticle degrading.

Table of Contents

List of Figures

List of Tables

Acknowledgments

I thank and am grateful for the mentorship my PI, Prof. Richard Friesner, over the 5 years of my thesis, and would like to thank the rest of my defense committee: Prof. Louis Brus, Prof. David Reichman, Prof. Angelo Cacciuto, and Prof. Barry Honig. I would also like to thank Dr. Michael Steigerwald for his counsel on certain aspects of this project, especially with the passivation schemes (along with Prof. Louis Brus, too). I'd like to thank Dr. Jing Zhang for the initial work he did for the initial guess fragmentation scheme for rutile, which we build off of for this work. Lastly, I'd like to thank Dr. Andrew Weisman with whom I worked on this project for the majority of my time at Columbia University who worked assiduously and whose help and work was indispensable. I deeply appreciate all those who helped me along the way.

Dedication

I dedicate this work to my parents, without whose help and support I wouldn't have been able to attend Columbia University and complete this dissertation.

Chapter 1: Introduction

In a photoelectrochemical water splitting solar cell, depicted in Fig. 1, the overall chemical reaction is

$$\textbf{(1)}\ 2\,H_2O \longrightarrow O_2 + 2\,H_2 \qquad \Delta E = 4.92\,eV$$

The source of the 4 × 1.23 eV = 4.92 eV of input energy is light, in which, nominally, one photon increases the potential energy of each of four electrons by 1.23 eV on average.[1] Typically, the anode consists of a mesoporous layer of semiconducting nanoparticles that absorb a photon to excite an electron across the band gap of energy E_g, thereby increasing the potential energy of the electron by E_g. Thus, the minimum nanoparticle band gap for a functioning cell is 1.23 eV.

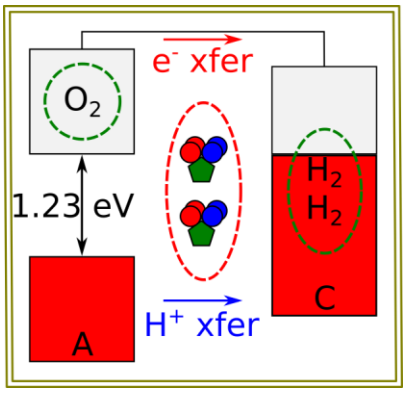

Figure 1 - Schematic of a water splitting solar cell, in which water is used up (red dashed border) and hydrogen and oxygen are formed (green dashed border) as the electrons increase in potential by 1.23 V. The representative materials and Fermi levels of the electrodes are shown using orbital energy diagrams: the anode is a semiconductor with a gap of at least 1.23 eV, valence band shown in red, and conduction band shown in gray; and the cathode is a metal, typically platinum, with the Fermi level shown by the intersection of the filled red states and empty gray states. In the water molecules, the red circles represent electrons, the blue circles protons, and the green circles oxygen atoms.

1.23 eV of input energy per electron transferred must be put toward increasing the potential energy of only one electron; any extra energy required for the cell to function is attributed to the "overpotential" of the cell. One of the most important questions to answer in the study of photocatalytic water-splitting in TiO_2 is to identify the large energy loss caused by the large overpotential associated with the reaction OER at the anode [2, 3]. To illustrate, were the band gap of the nanoparticle were equal to the free energy of the ideal water-splitting reaction, 1.23 eV, then the efficiency of the electrocatalytic cell is 41% [4]. Typical sources of overpotential in semiconductor-based photoelectrochemical cells include resistance in the external wire through which the electrons travel, inefficiencies in the proton transport/hopping through the electrolyte (nominally water) [49], poor charge separation/recombination of electrons and holes in the nanoparticles [6-13], and, as is the focus of this work, unstable intermediate species [3, 14, 15] at the surfaces of the nanoparticles during the OER.

In a working photoelectrochemical cell, eq. 1 is broken up into the OER occurring at the anode and the hydrogen evolution reaction (HER) occurring at the cathode:

$$\textbf{(1a)}\ OER\colon 2\,H_2O\ +\ 4\gamma\ \longrightarrow\ 4\,e^-\ +\ 4\,H^+\ +\ O_2\ +\ \Delta E_{OER}$$

$$\textbf{(1b)}\ HER\colon 4\,e^-\ +\ 4\,H^+\ \longrightarrow\ 2\,H_2\ +\ \Delta E_{HER}.$$

Here, four photons γ are added to the reactants in order to explicitly state the input energy source that provides the required 4.92 eV of energy; with these photons explicitly present in the equations, there is no need to include $\Delta E = 4.92$ eV to the right of the equations. Ideally, powered by these four photons, the water splitting would then proceed unassisted, i.e., there

would be no overpotential in the cell and $\Delta E_{\mathrm{OER}} \leq 0$ and $\Delta E_{\mathrm{HER}} \leq 0$. If $\Delta E_{\mathrm{OER}} > 0$ or $\Delta E_{\mathrm{HER}} > 0$, then these energetic requirements for water splitting would be attributed to the overpotential.

While other mechanisms have been proposed [16-18], it is typically assumed by most in the field [14, 19, 20] that the OER proceeds via four PCETs, each of which begins with a nanoparticle absorbing a photon to create a free electron in the nanoparticle's conduction band and a free hole in its valence band. Describing the nanoparticle + adsorbate by ${}^{*}\mathrm{A}_i\mathrm{H}$, where * is the nanoparticle with the reaction site unpassivated and $\mathrm{A}_i\mathrm{H}$ is the adsorbed surface species at the start of PCET i, then the photoexcitation is described by

$$\textbf{(2)}\ \gamma\ + * A_i H \longrightarrow (e^- + h^+ + * A_i H).$$

The energetic requirements for this process are $E_\gamma \geq E_g \geq 1.23\mathrm{eV}$, and, as our focus is elsewhere within the OER, we assume that these requirements are satisfied.

We likewise assume that electron-hole recombination, exciton formation, and electron trapping and hopping are all insignificant and that the conduction band energy is greater than or equal to the Fermi level of the cathode so that the transfer of the electron from the anode to the cathode occurs spontaneously:

$$\textbf{(3)}\ (e^- + h^+ + * A_i H) \longrightarrow (h^+ + * A_i H)\ + e^- .$$

Thus, at the beginning of each of the four PCETs of the OER, the nanoparticle at the anode, $(\mathrm{h}^+ + {}^{*}\mathrm{A}_i\mathrm{H})$, has a $+1e$ charge (it is "cationic") due to the presence of the hole. We

further ignore how the electron and hole transfers occur after they are created by the photon and assume that the cationic nanoparticle at the beginning of each PCET is in equilibrium and is thus fully geometrically relaxed.

Thus, adding **eqs. (2)** and **(3)**, each photoexcitation step is described by

$$\gamma \; + * AiH \longrightarrow (h \; + \;\; + * AiH) \; + \; e^{-} \;\; ,$$

each of which is followed by a PCET of the form

$$\textbf{(4)} \; (h^{+} + * A_i H) \longrightarrow * A_i \; + \; H^{+} \, .$$

Note from this form of the PCET that the "Electron" referred to in "PCET" is the one originally belonging to the H atom in the surface species A_iH (see eq. 7 for an example of this explicit dependence). Likewise, the "Proton" (the H^+) is the one originally belonging to the same H atom. In a PCET, the electron and the proton from the H atom move in different directions; as will be shown in Section 4.2, while the proton transfers away from the nanoparticle onto an explicit solvent water molecule, the electron transfers into the nanoparticle.

Before the first and third photoexcitations, a solvent H_2O adsorbs to the reaction site on the nanoparticle surface, and after the fourth PCET, an O_2 desorbs from the reaction site. The surface species typically assumed, and generally experimentally verified [2, 3, 15], are

$$A_1H = OHH$$

$$A_2H = OH$$

$$A_3H = OOHH$$

$$A_4H = OOH.$$

Putting it all together, the 11 steps of the OER are:

(5) Adsorption 1: $* + H_2O \longrightarrow *OHH$

Photoexcitation 1: $\gamma + *OHH \longrightarrow (h^+ + *OHH) + e^-$

PCET 1: $(h^+ + *OHH) \longrightarrow *OH + H^+$

Photoexcitation 2: $\gamma + *OH \longrightarrow (h^+ + *OH) + e^-$

PCET 2: $(h^+ + *OH) \longrightarrow *O + H^+$

Adsorption 2: $*O + H_2O \longrightarrow *OOHH$

Photoexcitation 3: $\gamma + *OOHH \longrightarrow (h^+ + *OOHH) + e^-$

PCET 3: $(h^+ + *OOHH) \longrightarrow *OOH + H^+$

Photoexcitation 4: $\gamma + *OOH \longrightarrow (h^+ + *OOH) + e^-$

PCET 4: $(h^+ + *OOH) \longrightarrow *OO + H^+$

Desorption: $*OO \longrightarrow * + O_2$.

Aside from that provided by the four photons γ, if any of these steps requires energy, i.e., has an overpotential, then the OER will not proceed spontaneously and more energy will therefore need to be supplied for the reaction to proceed.

Chapter 2: Background

Renewable energy sources will only become increasing important as unrenewable fossil fuel reserves deplete and climate change exacerbates, necessitating the development of clean, noncarbon-emitting renewable sources of power generation [21]. Wind, and solar energy sources are lead candidates, as they don't pollute when harnessed for energy and the source of their energy is easily accessed and infinite. Due to their intermittent nature, properly robust energy storage capacity must be developed to store enough energy to meet demand even during off-times.

Molecular hydrogen, H_2, is a promising clean, replenishable fuel source and energy storage possibility. It can be generated by harnessing sunlight via photocatalytic water splitting and a proper catalyst to make the reaction possible.

The promise of water splitting for the production of hydrogen gas as an energy source [22] and energy storage [23] is well-documented. In short, if the energy required for the process $2\ H_2O \longrightarrow O_2 + 2\ H_2$ is provided by the sun, the resulting H_2 can be endlessly produced, transferred, and burned with O_2 to produce useful energy, with the only by-product being H_2O, which itself is useful, for example, in areas experiencing drought. Moreover, molecular hydrogen has the highest specific energy content as compared to competing energy carriers such as electricity and biofuels, other renewable sources like wind and biomass, and even traditional carbon-based fuels [12, 24]. The benefit to society of such an energy-dense, renewable material as a ubiquitous fuel source and energy carrier whose only waste product is water is difficult to overstate.

However, it has been found that water splitting is not yet economically viable due to an inefficiency in a subreaction of the overall water splitting reaction called the oxidation evolution reaction (OER). As the OER typically requires charge separation, it is often performed on the surface of a catalyzing material that fosters this separation of charge. Catalyst surface area can be maximized by using micro-sized clumps of nanoparticles; thus, efforts to increase the efficiency of the OER have often been focused on modifying the chemical makeup, size, and shape of the nanoparticle catalysts used.

The prototypical catalyst is TiO_2 in the rutile polymorph, which was that used in the first successful demonstration of water splitting in 1972 by Fujishima and Honda [25]. Since then, it has been proposed that using TiO_2 nanoparticles in the anatase polymorph with high exposure of the (001) surface would improve OER performance [6, 26, 27] due to longer carrier lifetimes [10] and higher electron mobility [28] comparatively. At the same time, it has been found that the OER requires less energy when it occurs at the steps in a terrace-step surface structure [29, 30] or at edges [31] at the intersections of surfaces, which have similar physical properties as steps.

This dissertation aims to explain the source of the overpotential oxygen evolution reaction occurring at the (001) surface of TiO_2 nanoparticles at an atomic level. In particular, we aim to provide a detailed mechanistic understanding of the proton, electron, and hole transfers involved in the OER's bottleneck process, the first of its four proton-coupled electron transfers (PCETs), due to the relatively unstable OH species left on the surface.

To do so, after reviewing the relevant physical concepts in Section 3.1, in Section 3.2, we built large (001)-exposing anatase TiO_2 nanoparticles from scratch, passivated them appropriately for the aqueous environment they react in, and then optimize their structures using

simulation methodologies that are at least as faithful to experiment as we have found in literature: hybrid DFT (B3LYP), an atomic orbital-based basis set (LACVP), and both implicit and explicit solvent models. We show that we obtain nanoparticle geometries and electronic properties that agree well with previous experimental and computational results. We further present a least-squares method for calculating the "ionicity" of the eight unique types of bonds in our system using the atomic charges from Mulliken population analyses, finding in particular that Ti atoms at the (001) surface receive negative charge from surface-adsorbed waters while giving negative charge to bulk O atoms. Achieving these geometries and associated wavefunctions allowed us to move on to simulating the first PCET of the OER through a series of fixed geometry optimizations.

We performed detailed simulations of the first PCET of the OER by explicitly pulling a proton off a water molecule adsorbed to the (001) surface to a nearby solvent water, and then continuing to pull the resulting hydronium ion away from the nanoparticle surface. To do so, about a dozen points along that reaction coordinate were chosen and the system was optimized at those points while freezing the adsorbate oxygen atom and explicit hydronium ion oxygen atom in space to lock in the reaction coordinate. Atoms more than 10 Å away from the reaction site were frozen as well, in order to make the optimizations inexpensive enough to complete in a tractable amount of time; these atoms are far enough away from the reaction region of the system to have negligible effect on the optimization. Using the same methodologies as for the nanoparticle optimizations, we obtain good agreement with previous work for the total amount of energy required for the PCET to proceed, i.e., the kinetic overpotential. Further, we find the PCET actually requires more energy when it occurs at an edge of the (001) surface than in the middle of the surface, in contrast to the finding that the overpotential is smaller at steps and

edges than on surfaces [32]. In addition, we find the PCET requires more energy on uncharged, hole-free versions of the nanoparticles, in agreement with previous findings showing that holes tend to catalyze the PCET [33-35].

Having found good overall agreement with previous experimental and computational studies for both the nanoparticle properties and the first PCET of the OER, in Section 4.3 we take a step back and ask how the proton, electron, and especially the hole involved in the PCET can inform these results. We consider the implications of our finding that throughout our simulations of the PCET, the hole does not interact with the transferring electron at all. We resolve this with our finding that the hole, at least in the optimized nanoparticles, is not nearly oxidizing enough to capture the electron. All of these results are put together to provide a plausible answer as to the source of the overpotential observed in the OER and changes that could be made to the system to minimize it.

Chapter 3: Modeling TiO_2 Anatase Nanoparticles

Before we could study the kinetics of the first PCET of the OER catalyzed by titanium dioxide nanoparticles, we first needed to construct the nanoparticles and optimize their structures using first principles methods. In order to do that, a new methodology to generate the initial guess was required to handle nanoparticles as large as the ones we sought to model were. Our group has previously developed an accurate methodology for modeling titania nanoparticles [36], in which all aspects of the problem are treated at least as realistically as throughout literature, and we think that applying this methodology to our problem here is apt and provides a better understanding of the system for the field in addition to the TiO_2 structures we used to study the OER.

We use density functional theory (DFT)-based methods to model the nanoparticles we create and obtain energies and structures of the ground state. We note that using DFT-based methods, where a localized Gaussian basis set positioned at each atom is used to expand the Kohn-Sham orbitals and an auxiliary plane wave basis set is used to describe the electron density to describe the orbitals, has been shown to be appropriate for large-scale DFT simulations [12, 37]. Use of semiempirical functionals employing pure generalized gradient approximation (GGA) can be useful for pure metal systems [37] but fail to model accurately the electronic properties of metal oxide systems, ultimately stemming from incomplete cancellation of the Coulomb self-interaction in the GGA functionals [38]. The use of hybrid functionals, like B3LYP, overcomes this shortcoming by mixing exact exchange from Hartree-Fock exchange and correlation from GGA [39]. Although this is more computationally expensive, accuracy of the simulations increases. We note here that we don't expect the band gaps obtained herein to compare particularly well with experiment: in addition to finite-size-effect considerations [40],

the use of hybrid functionals to model metal oxides are known specifically to overestimate the bandgap of these semiconductors [32, 12]. Despite this, we otherwise expected our results agree well with experiment and theory, giving us a confident starting point for the PCET simulation.

3.1 Cutting TiO_2 Anatase Nanoparticles from Their Bulk Structure

To proceed with our experimentation, 3D models anatase TiO_2 nanoparticles were made by obtaining the coordinates of bulk anatase TiO_2 atoms from the Cartesian coordinates of the atoms in the unit cell from a high-quality submission (#63711) in the ICSD Web database [41] and copying them in all three spatial directions in MATLAB.

While the anatase crystal structure is shown be the most reactive polymorph of TiO_2 [6, 26-28, 42, 43], which surface is more catalytically active has been subject to debate. There are two primary surfaces of the anatase TiO_2 nanoparticle – the (101) surface and the (001) surface. In recent years, there has been an increase in experiments [44-48] focusing on synthesizing TiO_2 anatase nanoparticles that predominately expose the (001) surface, owing to earlier experiments suggesting that it is the more reactive catalytic surface [6, 14, 36, 49-52] owing to its larger conduction band edge energy [8, 53]. Ultimately, we choose to study this surface in order to be able to study the first PCET of the OER – as will be discussed in Section 3.2, this surface is passivated by water molecules, the adsorbate reactant of the first PCET, whereas the (101) surface is passivated by hydroxyls, the adsorbate reactant of the second PCET. Additionally, anatase TiO_2 is the most stable polymorph at the size of the nanoparticles we seek to model [54].

In order to create nanoparticles in the Wulff-constructed, experimentally-verified truncated bipyramid structure that exposes two (001) surfaces (top and bottom) and eight (101) surfaces (sides), unique cuts along the corresponding directions were made by (1) ensuring the exposed

atomic planes were auto-compensated and non-polar [55] (i.e. ensuring the number of Ti – O and O – Ti cuts are equal so as to retain neutral surface charges everywhere), and (2) choosing those that required cutting the fewest bonds per unit area. The first criterion defined the cut to be made in the <001> direction well, but left which cuts could be made in the <101> direction ambiguous. The second criterion would generally lead to the lowest-energy cut of the bulk and, importantly, defined the cut needed to be made in the <101> direction well. This results in nanoparticles of chosen dimension and shape liberated from its bulk structure. We were able to create a catalog of anatase TiO_2 nanoparticles of different sizes and shapes that exposed the correct atomic planes. We verified our nanoparticles by viewing the structures of titania anatase nanoparticles in literature and comparing them to ensure they were the same. The shapes of some nanoparticles were "sharper" than others, revealing relatively more of the (101) surface (Fig. 2, left) than on "flatter" nanoparticles, which expose a larger proportion of the (001) surface (Fig. 2, right). Both of these images show these nanoparticles passivated with water-derived ligands; the process we followed to do so is described in the next subsection.

3.2 Explicit Passivation of Nanoparticle Surfaces with Water-Derived Ligands

The next step in building up our TiO_2 nanoparticles to use in simulation was to appropriately passivate the exposed surfaces of our nanoparticles realistically in a water-splitting setting. Proper passivation of the nanoparticle is crucial – water adsorption substantially lowers the potential of the first PCET by as much as 0.7 eV [17]. Unable to find a well-justified consensus in the explicit passivation schemes in literature, we formulated our own by ensuring that the oxidation states and coordination numbers of the atoms were as satisfied as possible. In bulk anatase TiO_2, each Ti atom is coordinated to six O atoms, and to achieve noble gas valence,

Ti generally wants to give away its four valence electrons. Thus, four of the six Ti–O bonds in bulk are covalent, with one Ti atom contributing one electron to each. Similarly, in bulk each O atom is coordinated to three Ti atoms and generally wants two more valence electrons, so two of the three O–Ti bonds in bulk are covalent, with one O atom receiving one electron from each. This satisfies the oxidation states of the Ti and O atoms in bulk. The remaining two out of six bonds from each Ti atom and one out of three bonds from each O atom are donor-acceptor bonds in which, for each bond, the O atom "donates" a pair of electrons to the Ti "acceptor."[1] In this way, the coordination numbers of the atoms in bulk are satisfied as well.

Cleavage between the appropriate atomic planes at the (101) and (001) surfaces as described above leaves dangling bonds in which the oxidation states and coordination numbers of some exposed atoms are left unsatisfied. On the (101) surface, there is a Ti species and an O species that are each missing one covalent bond, and on the (001) surface, there is a Ti species and an O species that are each missing one donor-acceptor bond. In the nominal water splitting environment, which we assume to be pH neutral water, three uncharged species are available to passivate these atoms: (1) H, which generally wants to give away its electron to become H^+, (2) OH, which wants to receive one electron to become OH^-, and (3) H_2O, which has a satisfied oxidation state but whose O atom is able to donate an electron pair as part of a donor-acceptor bond. We note that the neutral H and OH species come about from dissociative adsorption of H_2 O on the nanoparticle surface.

We therefore match the unsatisfied atoms on the surfaces with the species available from the solvent to passivate these atoms: on the (101) surface, the unsatisfied Ti species is passivated with neutral OH so the Ti has something to which to give an electron, while the unsatisfied O

[1] Using our "ionicity" analysis in Section 3.5, we actually find Ti to be the donor and O to be the acceptor.

species is passivated with neutral H so the O has something from which to take an electron. On the (001) surface, the unsatisfied Ti species is passivated with H_2 O so the Ti has something from which to accept an electron pair, and the unsatisfied O species is left unpassivated because there is no species from the solvent to which to donate an electron pair. The remaining unsatisfied species of Ti atoms located at the corners and edges between surfaces are passivated using similar reasoning. Fig. 2 shows two unoptimized nanoparticles using this passivation scheme.

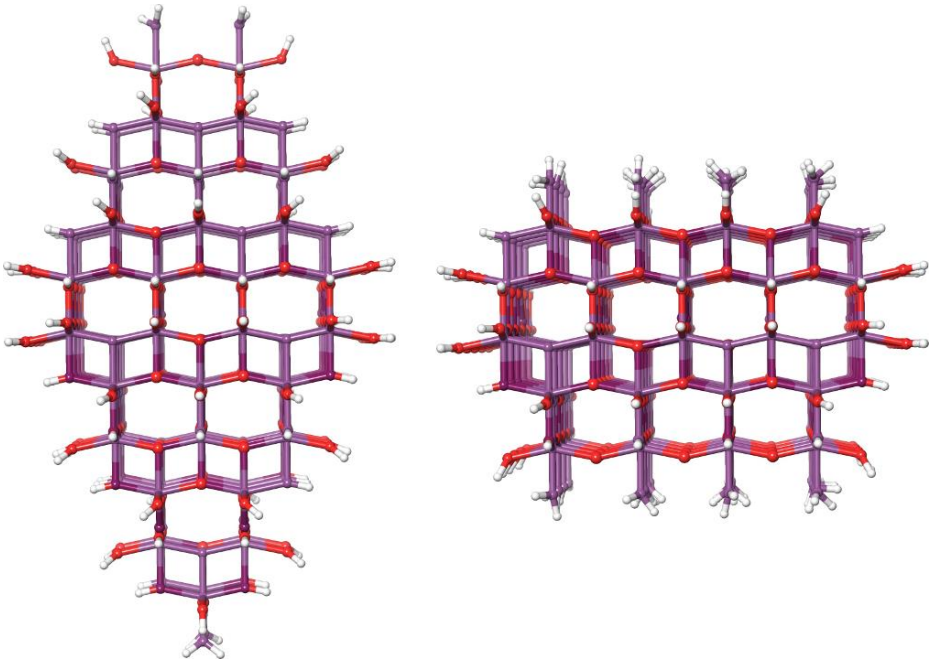

Figure 2 - Passivated, unoptimized nanoparticles. The one on the right corresponds to the “large” nanoparticle discussed in the text. The one on the left depicts a “sharper” nanoparticle with less (001) surface exposed than the one on the right. Dark purple atoms are artificial atoms that help the bonds display correctly in the Maestro software used for rendering the molecules.

We note here that it is somewhat common in both theoretical [1, 14, 55] and experimental literature to have dissociative water adsorption on the (001) surface and molecular water adsorption on the (101) surface, but according to the simple electron-counting rules we’ve

assumed, such passivation schemes are unreasonable. Future studies could include testing this passivation scheme anyway, but in the meantime, the current scheme is not only reasonable according to these rules but is also found to lead to an energetically stable nanoparticle, as will be shown Section 4.3 using first-principles simulations. This result in and of itself is significant: a correct passivation scheme is crucial of any computational-based study of these systems. Take the original, erroneous passivation scheme we tried versus the one that ultimately worked – the difference between the two is only the addition of H atoms on the O_{2c} atoms defining the edge between the (001) and (101) surfaces. With that tweak, we see in Figure 3 that the optimized large nanoparticles go from optimizing to a deformed, warped nanoparticle geometry to optimizing to a geometry that maintains the integrity of the nanoparticle structure.

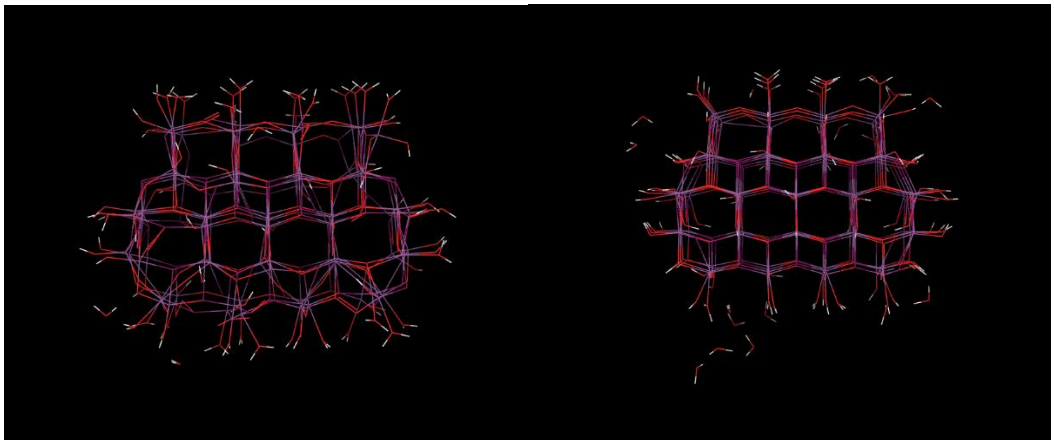

Figure 3 - Visualizations of two large nanoparticle geometries, one (left) with the incorrect passivation originally attempted, and one (right) with the correct passivation, achieved by adding H atoms to the O atoms defining the edge between the (001) and (101) surfaces.

3.3 Optimizing the Nanoparticles Using Density Functional Theory

In order to optimize the geometries of the anatase TiO_2 nanoparticles described in the previous subsection and to eventually carry out our simulation of the first PCET of the OER on

the surfaces of these nanoparticles using density functional theory (DFT), we needed good initial guesses of the wavefunctions. However, for any of the nanoparticles larger than 58 atoms in size (i.e. any of the nanoparticles even approaching realistic size), none of the initial guesses built in to Jaguar (the electronic structure software we use for our DFT calculations) specifically to handle systems containing transition metals resulted in converging self-consistent field calculations. To solve this, we used the Fragmented Initial Guess (FIG) algorithm with a general atomic partitioning scheme, developed by Prof. Friesner and previous group member Dr. Jing Zhang [36]. However, we could not use this code as-developed because the physical partitioning scheme it employed only worked for rutile polymorphs. Thus, we developed our own general partitioning scheme able to work on an arbitrary nanoparticle.

It is well-known that molecular systems that contain transition metal atoms exhibit complicated electronic structures due to their d-manifold being partially or fully occupied. As such, calculations of the electronic structure of these systems have proven difficult, and finding an initial guess good enough to have the optimization converge is certainly not trivial. Numerous methods have emerged for initializing of the quantum mechanical wavefunction needed for the self-consistent field (SCF) protocol that is paramount in any electronic structure calculation. Unfortunately, all such algorithms have failed for TiO_2 nanoparticles of both rutile and anatase polymorphs. As mentioned, Dr. Jing Zhang did produce a working algorithm to initialize the wavefunction of rutile TiO_2 nanoparticles, which worked by iteratively converging the wavefunctions of the fragments of a larger cluster, calculating the resulting charge fields of the fragments on their neighbors using a Poisson-Boltzmann solver, and re-converging the wavefunctions of the fragments in the presence of these charge fields. This approach, constituting the Fragmented Initial Guess (FIG) method, has proven successful in generating

initial guesses of the wavefunction for rutile polymorphs of TiO_2 nanoparticles that can further be refined using the SCF procedure without failing.

However, such an approach for successfully initializing the wavefunction requires careful partitioning of the cluster into individual fragments in the first place. The hard-coded scheme originally deployed by Dr. Zhang for rutile polymorphs of TiO_2 could not be used for the anatase polymorph because the partitioning of the rutile nanoparticle into sets of planes was done in such a way that is much more ambiguous for the anatase polymorph. Motivated originally in part by the fact that anatase the is the more reactive polymorph of TiO_2 for use as a cathode of an electrochemical cell, and more saliently, our overall aim to realistically simulate the first step of the OER of water-splitting on titanium dioxide nanoparticles, we set out to develop a fragmentation scheme that would work for TiO_2 anatase nanoparticles too and could be generalizable to any nanoparticle. Accordingly, the scheme needed to be based on general physical principles that could be applied to a general cluster. Indeed, our efforts were successful and we were able to create a fragmenting scheme [56] that allowed us to generate working wavefunctions for all of our desired nanoparticles, of both rutile and anatase polymorphs, including one (anatase) with 97 Ti atoms and more than 500 atoms total, which is the eventual focus of our PCET simulation study.

Our idea was to break the nanoparticle up into fragments that are individually as stable as possible so that the nanoparticle resembles a system of realistic—i.e., energetically favorable—smaller particles interacting with each other electrostatically. The logic is that the more realistic these interacting fragments are, the better our DFT methods will describe the system, as these methods have been tested on realistic molecular systems for decades.

We decided to form these low-energy fragments from basic units that themselves have the same crystal structure as the larger nanoparticle of interest. These basic units must have relatively low surface energies because they are themselves very small nanoparticles of a naturally forming crystal structure. For example, for anatase TiO_2 we decided to use as our basic unit the smallest constructible bipyramidal chunk of atoms taken from anatase bulk. It turns out that such a chunk is the linear O–Ti–O group of atoms.

Since the combination of two low-surface-energy units must itself yield a low-surface-energy unit (all exposed surfaces are still low-energy), we decided to use as our fragments in the FMO-INIT code clumps of the basic three-atom TiO_2 units, and we wrote a simple algorithm to break the non-passivated nanoparticle up into such fragments. We stipulated that: (1) each fragment consists of 34 to 99 atoms, (2) the last-formed nanoparticle fragment is at least 70% of the average size (in number of atoms) of all the other fragments, and (3) each fragment has a (# of O atoms)/(# of Ti atoms) ratio of at least 1.75. Finally, we set the last fragment to be the much-larger layer of passivating ligands.

In all of our runs of the FMO-INIT code on various-sized passivated anatase nanoparticles (through systems of 500 atoms and 5000 basis functions in size), fragmenting the nanoparticle using this algorithm always produced at least one initial guess wavefunction whose SCF calculation converged. This occurred even when all other initial guess methods in the latest versions of Jaguar, including those developed specifically for transition metal systems, failed. Thus, this new fragmentation scheme and FMO-INIT procedure has the potential to be extremely robust. Our expectation is that it can be applied to other complex condensed phase systems for which the standard initial guess approaches experience difficulty.

3.4 Optimizing Nanoparticle Geometries

3.4.1 Neutral Nanoparticles

Once we were able to generate anatase TiO_2 nanoparticles structures exposing different amounts of (101) and (001) surfaces and to obtain for them initial guesses sufficiently good not to have Jaguar fail outright, we then optimized increasingly large anatase TiO_2 nanoparticles, eventually building up to ones large enough to be of consequential size and warrant use of a supercomputer to calculate. The general protocol we used was as follows: after using the FIG algorithm to obtain an initial guess for the nanoparticle, we initially geometrically optimized the nanoparticle with the guess in vacuum (with explicit waters still passivating the cluster's surface, but no implicit solvent) with a limited number of geometric optimization iterations. At first, we would split this stage into two phases – a "loose" vacuum optimization followed by a normal vacuum optimization, with the difference being that we used a larger SCF density convergence threshold (keyword: dconv) and larger SCF convergence energy threshold (keyword: econv) for loose optimizations than in normal ones. When run, we would take the resulting structure and guess from the loose vacuum optimization to use as the start structure and guess for the normal vacuum calculation with stricter converge criteria. As we ran more calculations and became more familiar with running them on our system, we would come to find the loose vacuum optimization, and to a lesser extent the normal vacuum optimization, unnecessary to achieve a converged result. Consequently, not all systems underwent this stage.

After optimizing the geometry of a cluster in vacuum, we would then run a "properties" calculation to obtain better electronic properties of the cluster (while fixing the geometry of the system in place by setting keyword igeopt = 0). We iteratively refined the energy and electronic properties by allowing more SCF calculation iterations (keyword: maxit) than in the geometric

optimization (up to 300 versus 8), as well as printed the frontier orbitals to .vis files in order to visualize and locate them on the cluster. This stage was generally unproblematic.

After this stage, we would then take the nanoparticle and reoptimize its geometry in an implicit water solvent (keywords: isolv = 2, solvent = "water"). These calculations saw the solvated nanoparticles structurally become a little less rigid and a bit more "round" than they were in vacuum, but largely the same shape. Additionally, many molecularly adsorbed waters on the (001) surface desorbed, drifting around the nanoparticle loosely associated with it over the course of the optimization, but not ever re-adsorbing elsewhere. This observation supports experimental evidence in literature suggesting low coverage of the TiO_2 (001) surface with molecularly adsorbed water [14]. After the geometric optimization converged, we would recalculate the electronic properties as described for the analog vacuum case above. The visualization of these orbitals was useful for comparison to those of the neutral nanoparticles and to ensure the sanity of our results at this point. A review of this protocol and a table of keywords used at each calculation stage is provided in Appendix A.1.

3.4.2 Cationic Nanoparticles

The work-up of cationic nanoparticles was essentially the same as for the neutral nanoparticles but shorter, as we were generally able to eliminate the vacuum stages from the protocol. By this stage, the nanoparticles' guesses were well-converged enough already to not have to do a preliminary vacuum optimization to get them to work (not to mention the fact that the structures of the ionic clusters in vacuum would warp fairly significantly from what their structures in solvent would be, which wasn't true for the neutral nanoparticles). To start, the resulting geometry and electronic structure from the (neutral) solvent properties stage was taken

and made cationic[2] simply by changing the keyword molchg from 0 to +1. We then ran the geometry optimization calculation in implicit water solvent. The same level of molecular desorption of water from (and consequent relatively low coverage of) the (001) surface was observed on these cationic clusters as on the neutral ones.

As was done for neutral clusters, a solvent properties calculation was then run on the system to refine its electronic properties and visualize the frontier orbitals. Visualization of these orbitals was important for three reasons: (1) to compare the electronic properties of the neutral nanoparticle to its cationic counterpart, (2) to be able to decide which surface-adsorbed water on the (001) surface from which to abstract the proton during the eventual calculations of the first PCET of the OER wisely, and (3) to determine where the hole localized on the nanoparticle. We expected the hole to play an important role in the kinetics of the first PCET itself or in why there is a large overpotential associated with this reaction step, or both, thus characterizing the hole well was critical. As will be discussed in Section 4, we found that the localization of the hole occurs on a surface O atom (an O_{3c} atom in the medium cationic nanoparticle and O_{2c} in the large cationic nanoparticle). While this results in a noticeable surface construction in the cationic medium nanoparticle, qualitatively the structures of both nanoparticles otherwise remain the same. We believe the reconstruction to be an artifact of its smaller size or of freezing the bottom plane of Ti atoms, and we leave further discussion of this difference in Appendix A.3.

[2] Jaguar, the computational chemistry software used, makes the nanoparticle cationic by deleting the highest-energy electron in the system, i.e. the electron in the HOMO. In a real-life TiO_2 nanoparticle, an incoming photon will likely not excite the electron in the HOMO, but rather some other electron in the bulk of the nanoparticle it hits and has enough energy to excite. Higher-energy electrons will cascade down to occupy lower-energy orbitals, forcing the "hole" to rise to the surface of the valance band and of the literal nanoparticle [59, 76]. The electronic structure of the nanoparticle resolves itself orders of magnitude faster than the surface chemistry plays out, thus we don't expect this technicality to have an appreciable impact on our results.

3.4 Optimizing Jaguar for Use on STAMPEDE Supercomputer

In addition, accurate DFT optimizations on nanoparticles as large as those we sought to study were impractical on our local computing cluster, even using the cutting-edge, speed-optimized Jaguar DFT package utilizing the pseudospectral electronic structure method. We therefore compiled and optimized the latest Jaguar code on the STAMPEDE supercomputer to utilize both inter- and intra-node communications.

Dr. Jing Zhang had compiled and old, unlicensed version of Jaguar to work on the STAMPEDE supercomputer to run calculations on rutile TiO_2 to study the electron-trapping and transport properties in dye-sensitized solar cells in a tractable amount of time. We attempted to get the newest, licensed version of Jaguar set up on STAMPEDE so we could benefit from the improvements in the software, which would be particularly important for our large nanoparticles. However, as the Jaguar codebase had grown significantly in size since the distribution Dr. Zhang had originally compiled to use on STAMPEDE, making the code difficult to compile even on a single node not housed at Schrödinger, Inc., and since Schrödinger, Inc. had begun phasing out internode communications (i.e. MPI; currently Jaguar is designed to run on only a single node), this turned out to be a time-intensive, obdurate exercise. Therefore, with the assistance of Dr. Jerome Vienne at the Texas Advanced Computing Center at UT Austin, which hosts the STAMPEDE supercomputer, we eventually got Jaguar's full functionally working on STAMPEDE. Additionally, we were able to optimize the code for STAMPEDE's hardware using Intel's optimization tools, resulting in greatly improved performance with respect to speed. We leave out further details except to note that, after attempting to use the better-supported Open MPI and MPICH2 parallel libraries, we ultimately got internode communications implemented

using Intel MPI, which is designed for the Intel Xeon nodes that STAMPEDE comprises anyway.

We optimize the nanoparticles using a methodology at least as advanced as we have found in literature so far: fully quantum mechanical calculations using hybrid DFT (B3LYP), basis functions based on atomic orbitals (LACVP), and a continuum solvent model (Poisson-Boltzmann), in addition to the aforementioned explicit passivation of all surfaces. Utilization of an atomic orbital-based basis set is particularly important for describing nanoparticles as small as anatase TiO_2.

In preparation for our "pulling" experiments of Section 4.1 aimed at elucidating the overpotential of the first PCET of the OER, we optimized the geometries of both a "medium" nanoparticle (147 atoms total, 21 Ti atoms, 1217 LACVP basis functions) and a "large" nanoparticle (519 atoms total, 97 Ti atoms, 4868 LACVP basis functions) exposing primarily the (001) surfaces. Upon optimizing the geometries of both neutral structures, the bulk anatase structure remains qualitatively close to that of the initial, unoptimized MATLAB geometries, even near the surfaces. We conclude that our passivation scheme aimed at satisfying oxidation states and coordination numbers in a neutral water environment, discussed in Section 3.2, is thus quite reasonable, and the resulting surface passivation should therefore be considered for other experimental and computational studies of anatase TiO_2 nanoparticles.

While all exposed and unsatisfied atoms were initially passivated by water ligands present in a neutral water environment (100% passivation), upon optimization, many of the donor-acceptor-bonded waters adsorbed to the (001) surface quickly desorbed as the neutral geometry optimizations proceeded. Many studies of the coverage of water and its dissociation on anatase TiO_2 surfaces exist in literature [1, 32, 55, 57, 14, 58], and we therefore add our own

contributions given the caveat that we did not attempt molecular adsorption on the (101) surface and dissociative adsorption on the (001) surface due to this scheme being theoretically unreasonable: we find it viable in a neutral water environment that adsorption on the (001) surface is molecular and relatively low-coverage [14] and that adsorption on the (101) surface is dissociative and high-coverage (100%) with the correct 1:1 ratio of OH to H passivating species.

3.5 Ionicity Analysis

As we anticipated it being important for analyzing the results of the pulling experiment simulating the PCET of the OER on TiO_2 and the mechanism for the relationship between bond lengths and atomic charges summarized in Section 4.2, we performed a "bond charge" or "ionicity" analysis for the bonds in the medium and neutral nanoparticles. The goal is to obtain an understanding of how ionic the bonds are — a property examined in other studies of TiO_2 — including both the direction and the magnitude of the transfer of negative charge between two bonded atoms. In particular, from the Mulliken charges on the atoms in the DFT-optimized nanoparticle, we calculated the amount of negative charge given from one atom ("donating" atom) to the other ("accepting" atom) between two bonded atoms, under the assumption that before any bonds were formed, the charges on all atoms were zero[3]. Even with this assumption, there are significantly more bonds (i.e., unknowns) than atoms of known charge, so in order to drastically reduce the number of unknowns, we defined classes of bonds, e.g., covalent bond in the TiO_2 bulk, donor-acceptor bond in the bulk, Ti – O bond between a passivating H_2O and a Ti atom on the (001) surface, etc., resulting in eight types of bonds. We additionally defined some

[3] E.g., in the single neutral molecule A–B with atomic charges +x and −x, respectively, we say that after bonding, atom A has given x of negative charge to atom B, and we would denote this by drawing an indicator of negative charge at a fraction x of the way from A to B, along with some indicator of from which atom the negative charge originates, as shown in Fig. 3.

of the particular bonds (six, those surrounding the center Ti atom) in the system as their own classes in order to reduce overall error, and then by performing a least-squares fit we were able to calculate the bond charges in the system, the results of which are shown in Table 1 and Fig. 3. By using the results (the bond charges) to re-calculate the charges on the atoms, the RMS error is found to be 0.04*e*, with a worst absolute error of 0.13*e*.

While a general population analysis gives us an estimate of the total charge on each atom, the ionicity analysis described here allows us to incorporate which atoms are bonded to which in order to give us an estimate of the charge on each atom resulting from the particular types of bonds. For example, it is found that instead of each Ti atom giving each of its four covalently bonded O atoms one electron resulting in an oxidation state of +4 on the Ti as discussed in Section 4.1, the Ti atom actually gives each of these O atoms roughly 0.38e for a total oxidation state (and charge) of about 1.52e, not counting the additional contributions to the donor acceptor-bonded O atoms. We further find evidence of what was noted of interest in Section 3.2: Ti atoms give negative charge (about 0.10*e*) to donor-acceptor-bonded O atoms in bulk, but receive negative charge (about 0.07*e*) from donor acceptor-bonded waters on the (001) surface.

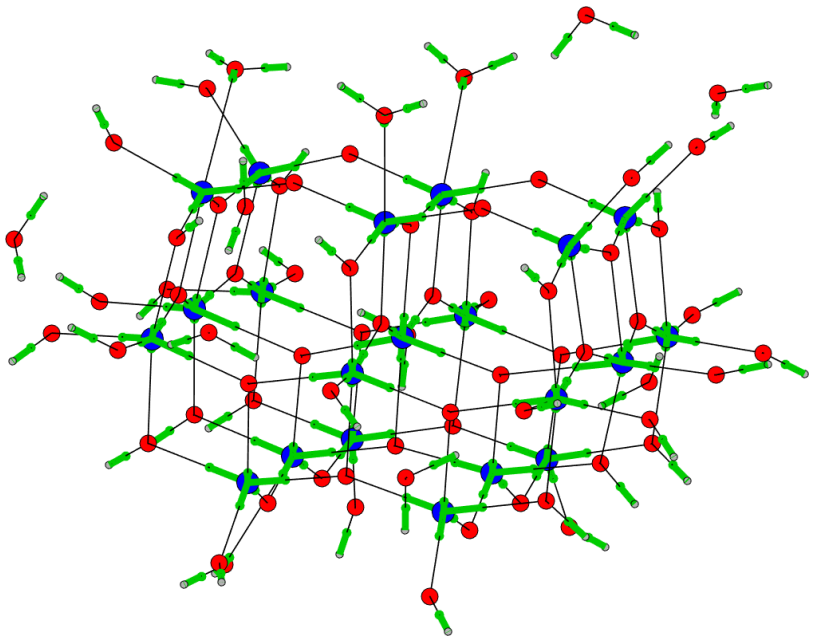

Figure 4 - Plot of the ionicity of the neutral medium nanoparticle. H atoms are small gray circles, O atoms are medium-sized red circles, and Ti atoms are large blue circles. Every bond has a green overlay indicating its ionicity, with the atom providing the negative charge shown by the start of the green line and the location of the negative charge shown by the end of the green line.

Bond class	**Bond charge (*e*)**	**Bond direction**
Covalent bond in bulk	0.38	Ti to O
Donor-acceptor bond in bulk	0.10	Ti to O
Covalent bond between O(101) and passivating H	0.42	H to O
Covalent bond between Ti(101) and passivating OH	0.29	Ti to O
O-H bond of a passivating OH	0.47	H to O
Donor-acceptor bond between Ti(001) and passivating H_2O	0.07	O to Ti
O-H bond of a passivating H_2O	0.42	H to O
O-H bond of a solvent H_2O (desorbed H_2O)	0.43	H to O

Table 1 – Ionicity properties of the eight main classes of bonds in the neutral medium nanoparticle, not including the similar values of the six one-bond classes, for which the largest difference is 0.09*e* and the bond directions are the same.

Chapter 4: Study of the First Proton-Coupled Electron Transfer (PCET) Step of the Oxygen Evolution Reaction (OER)

In order to study the kinetics of the first PCET as the likely source of the overpotential associated with the OER on TiO_2, we construct as best as possible the potential energy curve for the entire proton transfer, which we found to comprise two stages: the transferring of a proton from a surface adsorbed water to an explicit solvent water molecule, and the diffusion of this explicit water molecule (now a hydronium ion) away from the (001) surface. We simulate this proton transfer from the cationic nanoparticle (versus the neutral one) as a model of the electron transfer having occurred before the electron transfer and form the neutral nanoparticle as a reference. We note that pulling the proton from the neutral nanoparticle is most likely not an accurate representation of the proton transfer occurring before the electron transfer because the electron would be in a ground state, not an excited state. Additionally, were the electron excited and the proton transfer already occurred, we would not expect the electron transfer to occur as it would have relaxed down to the valence band where it would stay or alternatively become trapped in a state below the conduction band in the bandgap, as shown in [36]; in general, we do not expect the proton and electron transfers to happen in a particular order. To simulate a system where they happen simultaneously would be even more difficult, as it would necessitate modelling the cathode to which the electron is drained at the same time, in order to balance charge and multiplicity over the entire closed system.

4.1 Methodology

We simulated the kinetics of the first PCET of the OER, (h^+ + *OOH) → *OH + H^+, by "pulling" a proton, H^+, off of a water molecule molecularly adsorbed to the (001) surface of a cationic anatase titania nanoparticle. Originally, we attempted to abstract the proton away from the nanoparticle by itself, that is, without a "target" explicit water for it to bond with to form a hydronium ion. However, preliminary calculations trying to simulate the PCET in this manner were problematic for, among other things, difficulty achieving convergence and ambiguity over the proper van der Waals radius to use for the abstracting proton. Moreover, this is not the best representation of the actual PCET reaction we can achieve: bare protons only exist in water solvent fleetingly and are better understood as existing as part of a H_3O^+ ion. Thus, we chose instead to pull the proton directly to (or from) a nearby explicit "target" water molecule (or hydronium ion):

$$\textbf{(6)}\ (h^+ + *OOH) + H_2O \rightarrow *OH + H_3O^+.$$

Fig. 5 shows the setup of the pulling experiments we performed, depicting a medium nanoparticle with its reaction coordinate defined by the bottom plane of Ti atoms. Because the reaction of eq. 6 contributes to the overpotential and is thus energetically uphill, we choose a "pulling experiment" to be a series of geometry optimizations starting from the right-hand side of eq. 6 with the H_3O^+ starting at different distances from the nanoparticle, with the expectation that at some close-enough distance, the H^+ will spontaneously transfer from the hydronium ion to the *OH to from an adsorbed water ligand (we note that, chemically, we do not expect it to matter whether we simulate the PCET backward or forward by the principle of microscopic

reversibility). In each optimization, we fix the coordinates of the five Ti atoms at the base of the nanoparticle and of the O atom of the H_3O^+. Furthermore, the same nanoparticle geometry is used at the beginning of each optimization: the cationic nanoparticle with the transferring H^+ deleted from the adsorbed H_2O without further optimization. The H_3O^+ is then placed with the transferring H^+ above where it would be if it were still part of the adsorbed H_2O. Effectively, we are simulating the higher-energy (*OH + H_3O^+) configuration rather than the lower-energy (*OHH + H_2O) configuration as a function of distance away from the nanoparticle of the mobile H_3O^+/H_2O species[4].

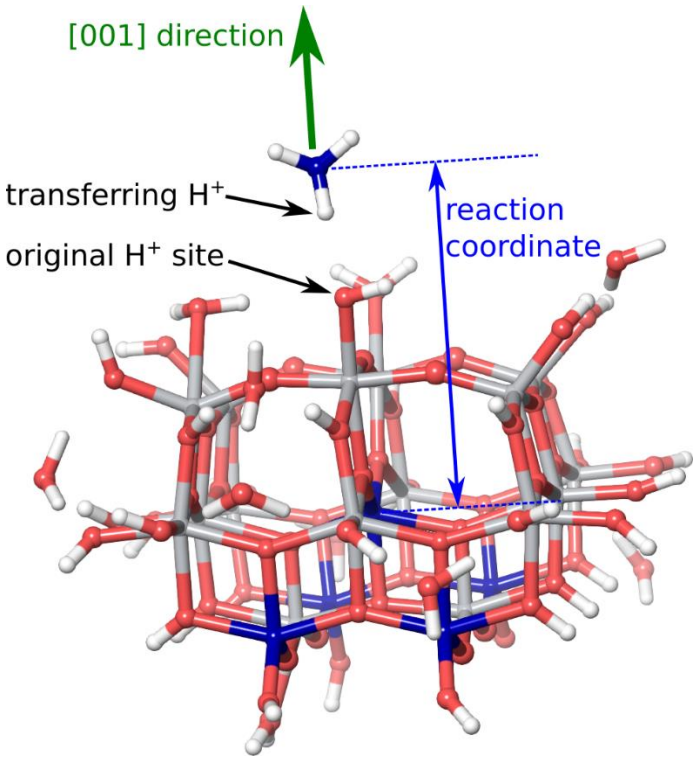

Figure 5 – Representative system configuration at the start of one of the geometry optimizations making up a pulling experiment. In each geometry optimization, the H_3O^+ is placed at a different distance from the nanoparticle and the system is optimized with the coordinates of six atoms (shown in blue) frozen in space. At sufficiently small values of the reaction coordinate, upon optimization, the H_3O^+ becomes H_2O as the transferring H^+ spontaneously transfers back to its original site as part of an adsorbed H_2O. While the particular system shown here is representative off the starting configuration for every geometry optimization of the medium

[4] Finite-temperature of transition state calculations would involve calculating a Hessian, which, for systems as large as ours, is impractical.

nanoparticle systems, it is actually the result of the 7.83 Å optimization of the cationic pulling experiment (with one of the desorbed waters deleted for ease of labelling for this figure). We note that for the large nanoparticle system, we start with an explicit water molecule nearby the nanoparticle and iteratively pull it away until the H^+ spontaneously transfers from the adsorbate H_2O to the explicit water molecule, making it a hydronium ion, and continue to pull away the hydronium ion from the nanoparticle to complete the PCET.

Our reaction coordinate is defined as the distance along the pulling direction from the topmost frozen Ti atom to the frozen O atom of the hydronium ion. We choose the pulling direction to be <001>, which, for cubic lattices like anatase, is the direction normal to the (001) surface We choose values of the reaction coordinate to best sample the potential energy curve obtained from plotting the total system energy vs. the reaction coordinate. The first values we selected were informed by preliminary linear and quadratic synchronous transit calculations we performed in order to home in on the location of the transition state. Further discussion of these jobs is left for Section 4.1.2.

As the process in eq. 6 is thought to occur more efficiently at edges between surfaces [29, 30], we further choose to isolate this variable by performing a pulling experiment on both a "surface"-adsorbed water ligand located as close as possible to the center of the top (001) surface and an "edge"-adsorbed water ligand located at the intersection of the (001) surface and a (101) surface, depicted in Figure 6. Further, as a baseline, we perform the same two pulling experiments on a neutral nanoparticle (before being made cationic and the hole forming), using the same surface and edge adsorbates as on the cationic nanoparticle, resulting in four total pulling experiments for this nanoparticle. As we only ran a "surface" pulling experiment on the large nanoparticle, and due to difficulties in keeping the system's waters adsorbed enough to converge, we leave discussion of the edge cases for Appendix A.

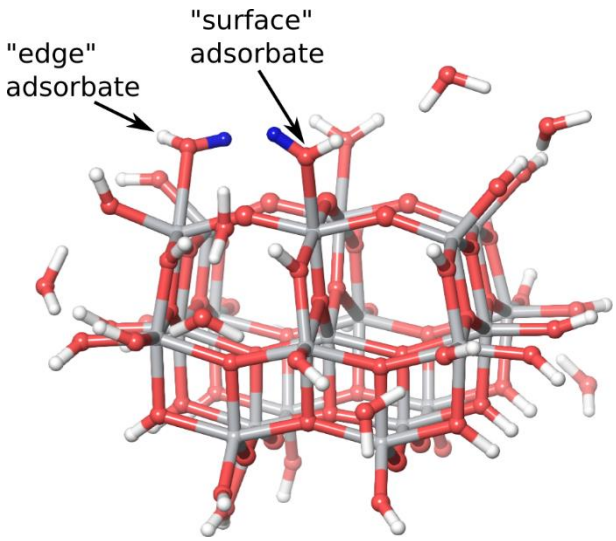

Figure 6 – Optimized cationic nanoparticle showing the two different surface-adsorbed waters on which the pulling experiments are performed. The transferring protons are colored in blue and labeled.

4.1.1 Addition of the "Target" Water Molecule

While the medium nanoparticles were small enough to be able to delete the H from the appropriate *OHH, add the explicit hydronium ion, and have the calculation converge, this was not possible for the large nanoparticle. Although desorbed water molecules generally occupied the environment around the nanoparticle, none were close enough nor in a proper orientation to bond to a proton pulled from the nanoparticle surface in a realistic manner. As such, we sought to add another water molecule to the system we had fully optimized in a position amenable to the PCET occurring. While the addition of one more water molecule to a system with already over 500 atoms (and 97 Ti atoms) is inconsequential to the overall properties of the system, the manual addition of the water molecule means we have to manually combine its wavefunction with the wavefunction of the fully optimized system (before adding the target water). In short, we wrote a script to combine the two wavefunctions together by converting the Jaguar input files to MATLAB .m files, reformatting them in MATLAB, combining the two wavefunctions, and

then printing the now-combined, single wavefunction to use in our PCET study – to combine the two wavefunctions directly (i.e. combining the &guess sections in their Jaguar input files) isn't possible, as simply concatenating the two is not the proper calculation of the combined wavefunction.

4.1.2 Placement of the "Target" Water Molecule

To place the target water molecule in the system for the abstracting H^+ to land on in the large nanoparticle system, we first considered that the proton would likely transfer to a water molecule near the nanoparticle's surface. We further surmised that the oxygen atom of this water molecule would be facing the nanoparticle surface, and its hydrogen atoms pointed away from it, otherwise the transferring proton would be blocked from approaching in a way favorable for bonding. With this in mind, we ran sample linear synchronous transit (LST) calculations on smaller TiO_2 clusters (61 atoms, ~500 basis functions) to home in on where the target water molecule is near the transition state of the reaction. The LST calculation linearly interpolates between the reactant and product and simply tries to find the maximum along this coordinate. As such, we defined the reaction coordinate to be defined as the direction normal to the surface of the nanoparticle we were studying; that is, the <001> direction. Taking the (cationic) nanoparticle plus water system as the reactant, and the nanoparticle plus hydronium system as the product, we performed an LST calculation to determine the transition state of this reaction along the <001> axis. Then, we took the resulting transition state structure and guess and used it to seed a subsequent quadratic synchronous transit (QST) calculation, in order to make sure our water placement would be proper and as precise as possible. The QST calculation differs from the LST calculation in that it additionally requires a third input structure, a transition state

structure and guess (which we obtain from a preceding LST calculation). Consequently, it is not confined to a linear path between the reactant and product: it can search for a maximum along an arc across the potential energy surface that connects the reactant and product, and for a minimum in all directions that are perpendicular to this arc. Thus, this method is more robust, sampling more of the potential energy surface than the LST calculation. The results of our QST calculation validated our intuition, revealing the transition state to be along the <001> direction we had predicted. It further revealed that the transition state occurs was the hydronium ion is diffusing away from the nanoparticle surface, not as the H^+ is in transit between either water-based molecule. To obtain the most useful data, we hoped to more densely sample the region around the transition state than, say, the product state plateau. This was particularly important because, despite the vast computational resource STAMPEDE afforded us, we calculated that we had enough allocation to sample about a dozen points along the reaction coordinate on the potential energy surface. Thus, these results allowed us to more wisely pick which points along the reaction coordinate we would choose to run calculations for on STAMPEDE, which was important because we didn't know precisely what distance to place the target water, nor where along the reaction coordinate the transition state was.

Last in our consideration in placing the target water molecule was where above the nanoparticle's surface to put it; there are multiple water ligands absorbed to surface Ti atoms from which the H^+ participating in the PCET could plausibly come in our larger nanoparticle systems. We chose to place the target water nearby a water ligand adsorbed to a surface Ti atom bonded to the surface O_{2c} atom where the hole localized from our optimization of the cluster described in section 3. We chose this because, barring any other, overriding consideration, we expected the hole to be involved in the PCET, as others in literature have found [16, 35], either

directly participating or indirectly by generating an electron-withdrawing environment locally, making the abstraction of a nearby water adsorbate's hydrogen atom more facile.

With the explicit water added to our optimized cationic nanoparticle system, and placed in a location amenable to the first PCET of the OER occurring, we proceeded to construct the potential energy surface (as a function of the reaction coordinate, defined by the distance between the nanoparticle's surface and the target water's oxygen atom) by optimizing the combined system at varying points along it.

4.2 Results

Qualitatively, in both cases we see the PCET occur in two stages: a first stage where the proton shuttles between the adsorbate water molecule and the explicit water molecule, and a second stage where the explicit water molecule (now a hydronium ion) is pulled away in a direction normal to the nanoparticle's surface. The hydronium generally still has an effect on the nanoparticle until it is pulled far enough away; the system doesn't simply equilibrate as soon as the proton shuttles to the explicit water molecule. It is important to model both stages of the PCET and not just the more obvious first stage; indeed, the system reaches its largest energy configuration in the second stage, after the proton has transferred to the target water molecule and after the resulting hydronium ion has been pulled a little bit away from the nanoparticle surface. We detail the results from the medium and large nanoparticle systems in the following subsections. For the medium nanoparticle, because the differences between the edge cases and their "surface" case counterparts are small, and because we only run a "surface" case for the large nanoparticle, we focus here on the "surface" case of the medium nanoparticle and leave

further analysis of the edge case in Appendix A. However, briefly, despite our expectation, there was little energetic difference between the edge and surface cases, and, if anything, the surface case was slightly lower in energy than the edge case. This may buttress other evidence [14] that OER photocatalytic ability varies little between TiO_2 surfaces and is not sensitive to local surface structure.

4.2.1 Medium Nanoparticle

Snapshots of the pulling experiments pulled on the system are shown in Fig. 7 for the medium cationic (surface) nanoparticle system. A pulling experiment was also done on a neutral nanoparticle, but we leave most discussion and analysis of its results in Appendix A as it was done largely as a baseline with respect to the cationic systems and did not produce any unexpected result. Moreover, we did not have a large neutral nanoparticle system to which to compare it like we do for the cationic version.

Corresponding significantly changing charges and bond lengths, in addition to the charges on the uninvolved Ti atoms (those far away from the reaction site), are listed in Table 2. In each subfigure, the left graphic in the snapshot shows how the charges of the atoms change over the course of the pulling experiment, relative to the system with no solvent water nearby, which is shown in the (a) subfigure. Similarly, changes in bond length are shown in the right graphic in each subfigure. Colorbars that quantify the changes in the charge and bond lengths are depicted in the last subfigure.

In Fig. 7, it can be seen that at distances depicted in snapshots (b) and (c), the reaction coordinate is small enough that the proton transfers back from the hydronium ion to the adsorbate water molecule from which it came, to the (*OHH + H_2O) configuration, whereas in

(d) and (e) it is large enough that the proton remains on the hydronium ion, in the (*OH + H_3O^+) configuration. Subfigures (b) and (c) depict the first and last snapshots, respectively, where the system is in the "two waters," (*OOH + H_2O) configurations; subfigures (d) and (e) depict the first and last snapshots, respectively, of the hydronium ion, (*OH + H_3O^+) configuration. The swap in configuration, the point at which the proton will transfer to the target water molecule and stay there, consequently occurs at some reaction coordinate distance between those depicted in (c) and (d). However, it is important to note that the peak of the barrier of the potential energy surface isn't located here – it lies at a reaction coordinate farther away than that shown in subfigure (d) but before (e).

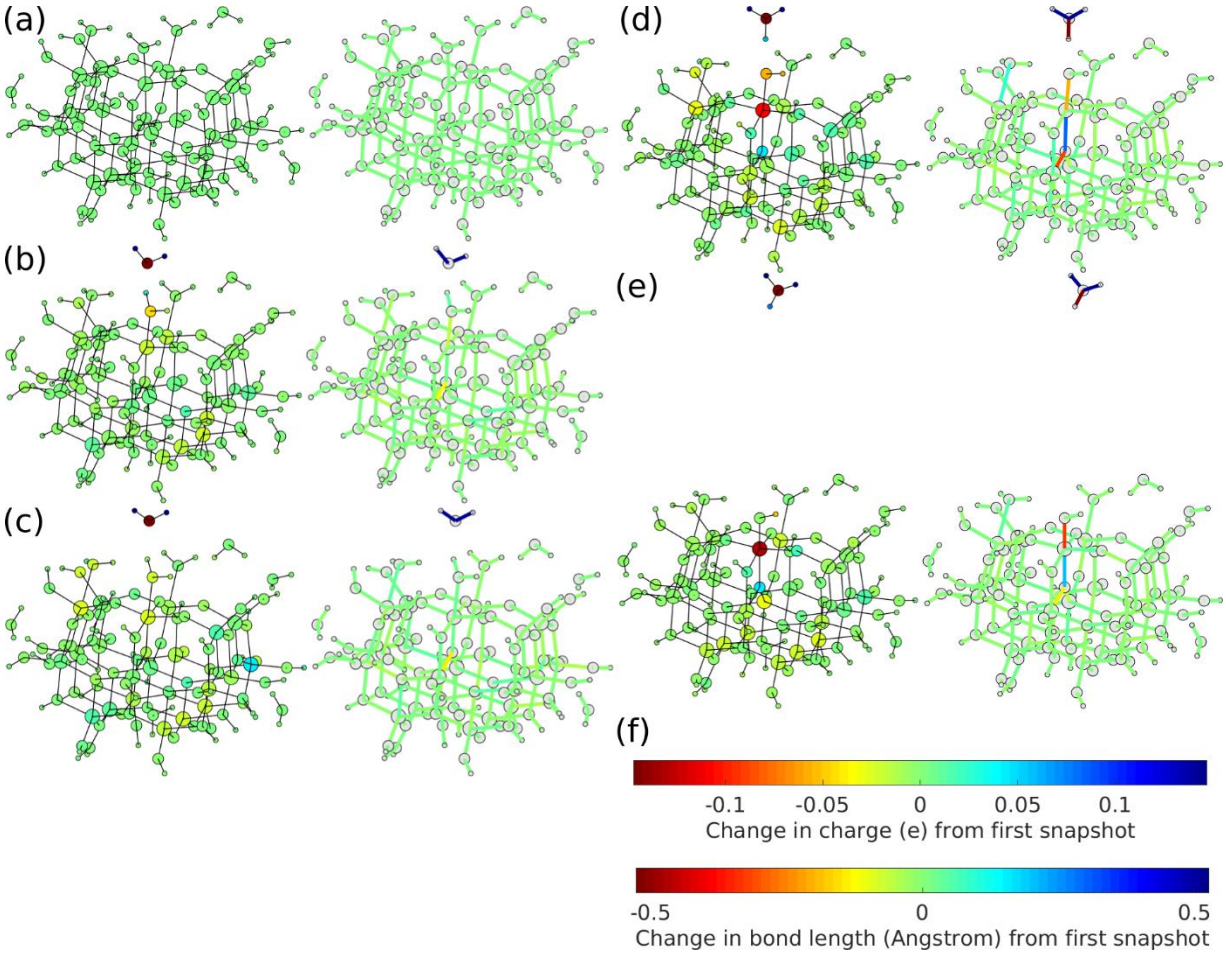

Figure 7 – Changes in charge (left of each subfigure) and bond length (right of each subfigure) for selected snapshots of the pulling experiment performed on the medium, cationic nanoparticle from a 'surface'-located (i.e. not edge-located) water adsorbate relative to the properties for (a) the cationic nanoparticle with no nearby explicit water added. (b) First datapoint of the pulling experiment; 7.03 Å. (c) Datapoint 3; 7.63 Å. (d) Datapoint 4; 7.73 Å. (e) Datapoint 17; 16.03 Å. (f) Colorbars describing the change in charge (top) and bond length (bottom) of the other subfigures. The numerical values of the important, significantly changing charges and bond lengths are listed in Tables 2 and 3.

Charges (e; cutoff=0.037*)*						
Atom name	**(a)**	**(b)**	**(c)**	**(d)**	**(e)**	**Notes**
Surface ads. H 1	0.47	0.50	0.47	0.53	0.55	Transferring H – surf.
Surface ads. H 2	0.47	0.46	0.46	0.41	0.42	Other adsorbate H – surf.
Surface ads. O	–0.74	–0.79	–0.77	–0.80	–0.75	Adsorbate O – surf.
Surface ring O 2	–0.81	–0.82	–0.82	–0.77	–0.77	Bottom DA O – surf.
Surface ring Ti 1	1.53	1.51	1.51	1.42	1.40	Surface Ti – surf.
Average uninvolved Ti	1.56	1.56	1.56	1.55	1.55	There are 20 of these

Table 2 – Significantly changing charges of interest during the cationic/surface medium nanoparticle pulling experiment. The corresponding plot of the changes in charge is shown in Fig. 7, to the subfigures to which the letter identifiers in the column headers refer.

*Bond Lengths (*Å*; cutoff*=0.079*)*						
Bond name	**(a)**	**(b)**	**(c)**	**(d)**	**(e)**	**Notes**
Surface Ti – O	2.22	2.16	2.24	2.00	1.88	Top DA – surf.
Surface Ring bond 2	1.87	1.90	1.90	2.19	2.09	Bottom DA – surf.
Close bond	2.76	2.64	2.62	2.44	2.62	
Edge Ti – O	2.37	2.35	2.41	2.45	2.40	Top DA – edge

Table 3 – Significantly changing bond lengths of interest during the cationic/surface medium nanoparticle pulling experiment. The corresponding plot of the changes in bond lengths is shown in Fig. 7, to the subfigures to which the letter identifiers in the column headers refer.

Snapshot (b) reveals that as the solvent water molecule is placed near the adsorbed H_2O (again, relative to (a)), the charge on the transferring proton increases from 0.47*e* to 0.50*e*, that

on the adsorbate's oxygen atom decreases from –0.74*e* to –0.79*e*, and that on the surface Ti atom to which it's bonded decrease from 1.53*e* to 1.51*e*.

The bond between the transferring H^+ and the adsorbate O lengthens from 0.98 Å to 1.01 Å and the bond between the adsorbate oxygen atom and the surface Ti beneath it shortens from 2.22Å to 2.16 Å.

These results could suggest a potential mechanism for the initial separation of charge required from the PCET to occur; as the negatively charged oxygen atom of the target water molecule pushes electron density off of the incoming H^+ (making it more positively charged) to remain on the adsorbate oxygen atom, making it more negative, it simultaneously pulls on the positively charged transferring H^+ itself. This results in the bond between the H^+ and adsorbate O lengthening, slightly weakening in consequently. It is important to remember that this in reference to a system with no explicit target H_2O placed nearby yet, not one where the water molecule is just closer to the nanoparticle surface – the mere addition of this water molecule changes the local charge and geometric arrangement of the system.

Snapshot (d) depicts the system just after the H^+ transfers to the target water molecule. As that happens, relative to snapshot (c) showing the system just before the H^+ transfers, the surface Ti atom moves upward toward the adsorbate, simultaneously shortening the top donor-acceptor bond from 2.24 Å to 2.00 Å and lengthening the bottom donor-acceptor bond from 1.90 Å to 2.19 Å. We posit that the (positively charged) Ti moves upward – as opposed to the entire adsorbate moving downward – because even though the H^+ has moved away, it is still close enough to the negatively charged adsorbate (whose negative charge decreased from –0.31*e* to –0.39*e* between snapshots (c) and (d)) to attract it fairly significantly, forcing the Ti attracted to it to migrate upward. Though subsequent snapshots of nearby points a little farther along the

reaction coordinate are not shown (i.e. snapshots between (d) and (e)), as the hydronium ion is pulled farther and farther away from the nanoparticle, the surface Ti atom – and therefore the entire adsorbate – settles backward down into the nanoparticle. This is likely due to the positively charged hydronium ion attracting the adsorbate increasingly little. Thus, the changing charges and bond lengths of the system gradually equilibrate to their final values, depicted in subfigure (e).

Subfigure (e) shows that after the H_3O^+ is pulled far away from the nanoparticle, the top donor-acceptor bond shortens from 2.00 Å to 1.88 Å, the bottom donor-acceptor bond shortens from 2.19 Å to 2.09 Å, and some negative charge flows from the adsorbate into the nanoparticle (0.06*e*). The Ti atom plus adsorbate moiety is allowed to relax back into the nanoparticle as the hydronium ion to which it (or at least the adsorbate *OH) is attracted continues to diffuse away from the nanoparticle surface.

The final atomic charges on the oxygen atom and hydrogen atom the adsorbate water comprises are similar to those of the OH species adsorbed to the (101) surfaces of TiO_2. Since the OH(101) species receives an electron from a covalent bond with a surface Ti atom (on the (101) surface) and can therefore be considered to be OH^- (a hydroxyl, not radical OH, ligand), we consider the resulting OH(001) adsorbate in our system to be a hydroxyl ligand too because the final charges of the constituent atoms are similar. However it is difficult to determine the type of bond the OH(001) species has with the surface: it could be donor-acceptor in nature in which the O atom of the closed-shell OH^- donates a pair of electrons to the surface Ti acceptor (just as the original adsorbed H_2O did), it could be covalent in which the negative charge that flowed onto the surface Ti atom is given back to the OH(001) species, or some mixture of the two.

4.2.2 Large Nanoparticle

Satisfied by the proof-of-concept the medium nanoparticle pulling experiment provided us, we then turned to studying the large nanoparticle. The pulling experiment of the large cationic nanoparticle (97 Ti atoms, 522 atoms, approximately 5,000 basis functions) we performed ultimately comprised optimizing the system at eleven points along the reaction coordinate. We studied only large cationic nanoparticle system pulling from a surface water adsorbate, and didn't perform analogue large neutral or edge nanoparticle pulling experiments, due to our finite computational resources for already such a large system. To further stretch our computational resources as far as we could, we froze all atoms more than ten angstroms away from the explicit water oxygen atom involved in the PCET, as well as that oxygen atom, too. Both the effects of adding the explicit solvent water molecule to the system and of making the nanoparticle cationic had negligible effect on these distant atoms in those optimizations; we don't expect the chemistry that the pulling experiment models to affect these atoms, either. Furthermore, in order to have a well-defined reaction coordinate for the PCET, we freeze the bottom plane of Ti atoms of the nanoparticle anyway so we can define the pulling direction as being the direction normal to this plane (on average). The reaction coordinate is then defined as distance along the pulling direction, starting from the plane formed by the four Ti atoms in the corners of the (001) surface (defined as zero) and ending at the explicit water (or hydronium) oxygen atom.

Given the size of our nanoparticle and the large computational expense each optimization would cost, we chose which points along the reaction coordinate to optimize with care. Ideally, we'd sample the area around the distance at which the system just becomes more stable in the

(hydroxyl + hydronium ion) configuration than the two waters configuration (i.e. the transition between the two stages of the PCET) more densely and also sample the transition state more densely. From the results we achieved with the medium nanoparticle, we discovered the approximate distance at which the H^+ finally transfers to the target water molecule (between 7.63 Å and 7.73 Å along the reaction coordinate in that system), and that the transition state lies a little bit beyond this point. This knowledge allowed us to sample the reaction coordinate wisely. The results of the pulling experiment largely align with those of the analog medium cationic nanoparticle experiment. The maximum of the PCET curve for the large cationic nanoparticle is 1.53 eV, with the difference in energy of the reactant and product being 1.08 eV (thermodynamic overpotential). This is in line with what we observed in our medium nanoparticle studies, validating our findings and suggesting that results obtained from smaller nanoparticles are able to be extrapolated to larger systems. This could save a lot of computational expense, however we are cautious due to other, qualitative difference which may undermine this suggestion (i.e. the reconstruction observed during the optimization of the cationic/surface medium nanoparticle, something not seen in the large case).

At small enough distances of reaction coordinate where the target water is very close to the nanoparticle surface, the H^+ is more stable on the adsorbate water molecule than the target water molecule (i.e. it is more stable as a two waters configuration). At this distance, if the starting configuration is (*OH + H_3O^+), the H^+ will shuttle from the hydronium to the hydroxyl to form two waters, the more stable configuration.

As the explicit water is pulled farther away from the surface, but still retaining the two waters configuration, the Ti – adsorbate O bond length lengthens by 0.08 Å as both moieties are pulled upward as the water occupies farther away reaction coordinates. Consequently, the bottom

donor-acceptor bond (between the surface Ti and the O atom beneath it) lengthens by 0.11 Å as the buried O atom is unaffected and stays in place. At a certain farther-out distance, the H^+ will stay on the target water molecule (forming a hydronium ion), as the system is at this point more stable in the (*OH + H_3O^+) configuration than the two waters configuration. As was found in the medium cationic nanoparticle studies, this point, when the proton finally shuttles to the target water for form a hydronium ion, while accompanied with a sizable increase in system energy, is not the maximum of the PCET. After this shuttling occurs, the surface Ti atom moves upward toward the adsorbate even more shortening the bond by 0.19 Å, and the bottom donor-acceptor bond to shorten by 0.19 Å. The change in bond length is caused by movement of the Ti upward – the adsorbate water-derived ligand remains in place, as does the bottom donor-acceptor O atom.

As the hydronium is pulled farther still from the nanoparticle, the total system energy continues to increase slightly until a maximum is reached, at which point the energy begins to fall as the H_3O^+ continues to diffuse away until it eventually plateaus. Notably, the Ti atom does not relax back down to where it was in the lattice before the pulling experiment started – it remains in its slightly elevated position out of its natural position in the surface. This appears due to lengthening of the bonds to either surface O_{2c} atom to which its bonded, which are now too long to allow the Ti atom to settle back down. The hydroxyl adsorbate however is allowed to settle down from its stretched-upward position during the proton shuttling back into the nanoparticle, causing the Ti – adsorbate O bond to shorten slightly as the plateau is reached by 0.06 Å.

Charges (e; cutoff=0.037*)*						
Atom name	**(a)**	**(b)**	**(c)**	**(d)**	**(e)**	**Notes**
Surface ads. H 1	0.47	0.51	0.49	0.52	0.55	Transferring H – surf.
Surface ads. H 2	0.48	0.47	0.48	0.43	0.44	Other adsorbate H – surf.
Surface ads. O	-0.75	-0.81	-0.81	-0.77	-0.75	Adsorbate O – surf.
Subsurface ring O 2	-0.92	-0.92	-0.91	-0.87	-0.87	Bottom DA O – surf.
Surface ring Ti 1	1.63	1.64	1.64	1.50	1.50	Surface Ti – surf.
Average uninvolved Ti	1.57	1.55	1.55	1.55	1.55	There are 96 of these

Table 4 – Significantly changing charges of interest during the cationic large nanoparticle pulling experiment.

*Bond Lengths (*Å*; cutoff*=0.079*)*						
Bond name	**(a)**	**(b)**	**(c)**	**(d)**	**(e)**	**Notes**
Surface Ti – O	2.22	2.03	2.11	1.92	1.86	Top DA – surf.
Surface Ring bond 2	1.96	1.99	2.10	2.29	2.29	Bottom DA – surf.
Close bond						

Table 5 – Significantly changing bond lengths of interest during the cationic large nanoparticle pulling experiment.

4.3 Discussion

4.3.1 Energetic Requirements of the OER

A plot of the total system energy vs. reaction coordinate distance for the medium nanoparticle systems and the cationic large nanoparticle system are shown in Fig. 8. Relevant values from the experiments are reported in Table 6 for comparison and discussion purposes. Results from a pulling experiment performed with a neutral medium nanoparticle are also included for the discussion and analysis of charge transfer kinetics taking place during the PCET.

	Medium neutral nanoparticle	Medium cationic nanoparticle	Large cationic nanoparticle
Overall *E* required	1.52eV	1.34 eV	1.53 eV
Thermodynamic overpotential (reactants minus products)	1.09eV	1.09 eV	1.08 eV
Kinetic contribution	0.44eV	0.25 eV	0.45 eV

Table 6 – Summary of the properties from the medium (surface) and large nanoparticle pulling experiments.

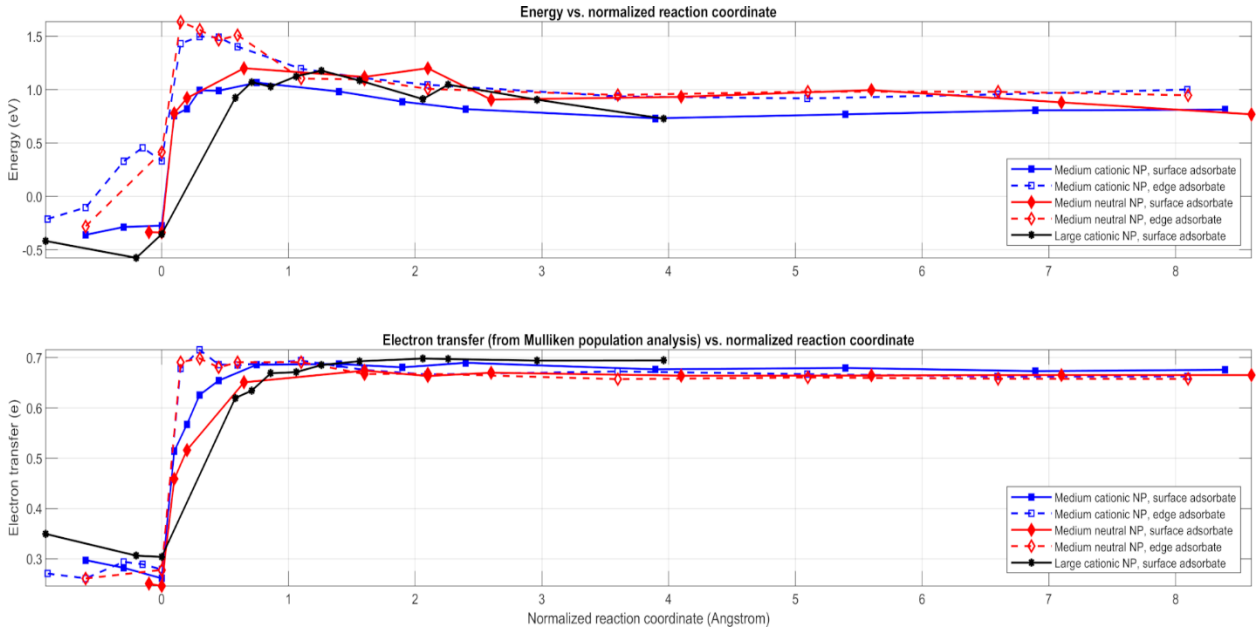

Figure 8 – (Top) Energy plotted as a function of reaction coordinate for the four medium nanoparticle systems and the large cationic nanoparticle system. Solid lines correspond to "surface" cases; dashed ones correspond to "edge" cases. The larger energies seen at earlier reaction coordinates for the edge cases is mainly caused by a water molecule continuously desorbing throughout the course of the experiment: see Appendix A.3.1 for further discussion. (Bottom) Amount of electron transfer as a function of reaction coordinate for the same systems.

From this plot and the values summarized in Table 6, we see that less energy is required of the PCET when the medium-sized system is cationic instead of neutral (1.52eV in the neutral system versus 1.34 eV for the cationic system). As will be elaborated on in Section 4.3.3, while this may be generally expected to be the case, we find that the ostensible reason explaining this phenomenon does not occur. The overpotential for the PCET on the large cationic nanoparticle system is similar at 1.53 eV. Interestingly, this data shows that even though it is ultimately the kinetics of the process (the maxima of the curves) that dictates the total energy required for the process, the thermodynamics of the process (captured in the high-reaction-coordinate values of the curves – the product plateau) shows that the degree of instability of the intermediate ∗OH species is independent of the charge of the system; the thermodynamic overpotential is found to

be about 1.09eV in both neutral and cationic medium nanoparticle systems. Additionally, this value is virtually the same as in the large nanoparticle system, showing remarkable invariance across the systems.

In literature, typical experimental OER overpotentials [2, 14, 19, 59-63] are found to be 0.6-0.8eV, while computationally obtained overpotentials tend to be a bit higher, around 1.1-1.4eV [14, 64, 65]. We note that there are differences between the reaction conditions between those that experimentalists widely use to study TiO_2's water splitting activity and those used in this work – chiefly, that they are studied operating under harshly basic or acidic conditions – making a direct comparison hard [66]. Additionally, overpotentials are typically reported as the overpotential necessary to drive a certain current density (typically 10 mA cm^{-2}), not at the current exchange density, meaning experimental data would overstate the overpotential relative to our study for a given system. On the other hand, computational results report overpotentials due primarily to the instability of the intermediate species generated at the end of the PCET – in this case, *OH – making for an easier direct comparison with our own study. Our results of an overpotential of 1.3 – 1.5 eV match up well with other computational results and we see we have obtained values in agreement with previous computational studies and are reasonable when compared to experimental results.

4.3.2 Electron Transfer

The transfer of the H^+ from the adsorbate to the solvent H_2O may be accompanied by the transfer of an electron from the adsorbate to the nanoparticle, as mentioned in Sections 4.1 and 4.2. This is one step of the oxidation that must occur at the anode of the photoelectrochemical cell. While the nanoparticle itself has already been oxidized since the cationization has given the

system a charge of +1*e* prior to the pulling experiments simulating the PCET, in order to return the nanoparticle to its initial electronic configuration so that the next step of the PCET can occur on a "reset" nanoparticle (the TiO_2 is catalytic), the hole from the cationization must be filled by an electron from the same adsorbate from which the H^+ transfer occurs. Considerations about filling the hole are discussed later in Section 5; here, we focus on quantifying the amount of negative charge that has left the adsorbate over the course of the pulling experiments.

We therefore calculate the "electron transfer" (ET) to the nanoparticle as the change in the total charge on the adsorbate and the solvent water molecule, which is equal to the negative charge transferred out of the (adsorbate + target H_2O) subsystem. However, the starting configuration of this subsystem is that in which its total charge is zero, i.e., before the adsorbed H_2O is even adsorbed to the nanoparticle surface, because this adsorption is the true first step in the full OER cycle, as shown in eq. 5. Thus, since the total charge on the adsorbed H_2O is not zero even before the nanoparticle is made cationic, we conclude that some electron transfer has already occurred before the start of the PCET by the proximity of the explicit water molecule. While most of this initial ET occurs upon adsorption of the H_2O, it should not be associated with the actual H^+ transfer; it is preliminary electron density transfer that is not part of the PCET.

In particular, the charge on the adsorbed water molecule in the medium neutral nanoparticle system is 0.19*e*; thus, the ET upon adsorption of the water molecule to the surface is 0.19*e*. Upon cationization, the change in charge of the adsorbate water is small, 0.01*e*. When an explicit water is added nearby this adsorbate, the negative charge on the adsorbate decreases by another 0.10*e* in the cationic system and 0.08*e* in the neutral system. Thus, the total ET in the medium neutral system is 0.27*e* and in the medium cationic system is 0.30*e*. For the large nanoparticle system, the charge of the adsorbed water ligand is 0.20*e*, which we take as the ET

before the PCET begins and agrees with what was observed in the medium nanoparticles. When the cluster is made cationic and an explicit water placed nearby, however, the sum of the charges of the atoms comprising the water adsorbate is 0.17*e*, constituting an *increase* in negative charge, albeit a modest one. We note that the change in charge with the addition of a nearby water may be somewhat dependent on the precise location and orientation of the water molecule; the next point along the reaction coordinate from the addition of the H_2O (where it is slightly farther away from the nanoparticle surface, but still close) shows the negative charge on the adsorbate water is slightly lower than the system with no water by 0.01*e*. While in both medium and large nanoparticles we see the preliminary electron transfer of the adsorbing water, it may be the case that the presence of another nearby, explicit water molecule forcing more e^- of the adsorbate and into the nanoparticle was unique to the medium-sized systems. Regardless, we acknowledge these findings here to more clearly delineate what processes are involved in the PCET and which are independent from it, as well as to contextualize the analysis of the role that the hole plays in the PCET and the overall OER, discussed next.

4.3.3 Role of the Hole

We have found that, unlike in some other studies [59], the ET discussed above is completely independent of the hole transfer; we find that the hole does not transfer at all and is stable throughout all of our cationic pulling experiments, localized on the same O_{2c} atom on the (001) surface. However, the decoupled nature we find for this PCET is supported by other work showing TiO_2 binds water weakly to its surface [67] and studies showing a decoupled mechanism is preferred in systems with weakly interacting surfaces [5]. It is in any event prudent to discuss the purpose the hole serves in the functioning of the water splitting solar cell. The

nominal role of the hole h^+ in the cell is twofold: (1) to capture the electron left behind by the transferring H^+ (i.e., the electron associated with the ET), and (2) to lower the energy required for the PCET.

Role #1 can be explicitly shown by adapting eq. 4 for the first PCET ($A_1 =$ OH) to include its dependence on the transferring electron e^-:

$$\textbf{(7)}\ (h^+ + [e^- + {}^*OHH +]) \longrightarrow ([{}^*OH]) + H^+$$

where the parentheses represent the entire cationic nanoparticle and the brackets represent just the relevant entities at the surface reaction site. This function of the hole is crucial to the functioning of a water splitting solar cell because, otherwise, at any given time there would be a number of holes present on the surface that would act as trap states for photoexcited electrons in the conduction band[5], preventing them from flowing out of the anode into the cathode. Another reason is that, otherwise, the OER would not be a cycle: at the end of the OER the nanoparticle would not be in the same state in which it began, as assumed in the subreactions of the OER shown in eq. 5. The TiO_2 nanoparticle must return to its original state for its catalytic cycle to complete. Instead, there would be a build-up of positive and negative charges throughout the nanoparticle as the electrons are unable to fill the holes due to their deficiently small energy. Further experimental and theoretical investigation would be required to learn the exact effects of this, but it appears that the electronic structure — and therefore likely the physical structure — of the nanoparticle catalyst would degrade and the reaction would be impossible to continue to occur.

[5] The hole lies 1.46eV below the LUMO in the medium nanoparticle and 1.26 eV below it in the large nanoparticle.

Role #2 of the hole has been found experimentally [16, 33]; holes have been shown to catalyze the OER. Assuming that role #1 is satisfied, it is natural that the hole would lower the energy required for the PCET because the hole would assist the electron transfer by giving the transferring electron a place to go. This would help the ET to be more in concert with the PT, in turn lowering the overall energy required for the PCET.

However, we have found that role #1 of the hole is not fulfilled: the ET transfer has nothing to do with the hole nor does the hole get filled by it. Instead, the properties of the hole remain very stable throughout all of our cationic pulling experiments. The hole orbital at the end of the experiments looks just as it did right after we first optimized the cationic nanoparticle (Fig. 9, for medium system; Fig. 10 for large system).

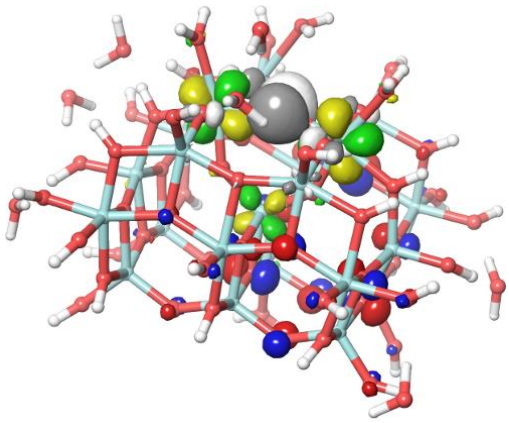

Figure 9 - Visualization of the hole (gray and white orbital) localized on reconstructed O_{3c} atom at beginning of pulling experiment of a medium cationic nanoparticle. The character and location of the hole is unchanged from the start of the pulling experiment. The LUMO and HOMO are also visualized in green and yellow, and blue and red, respectively.

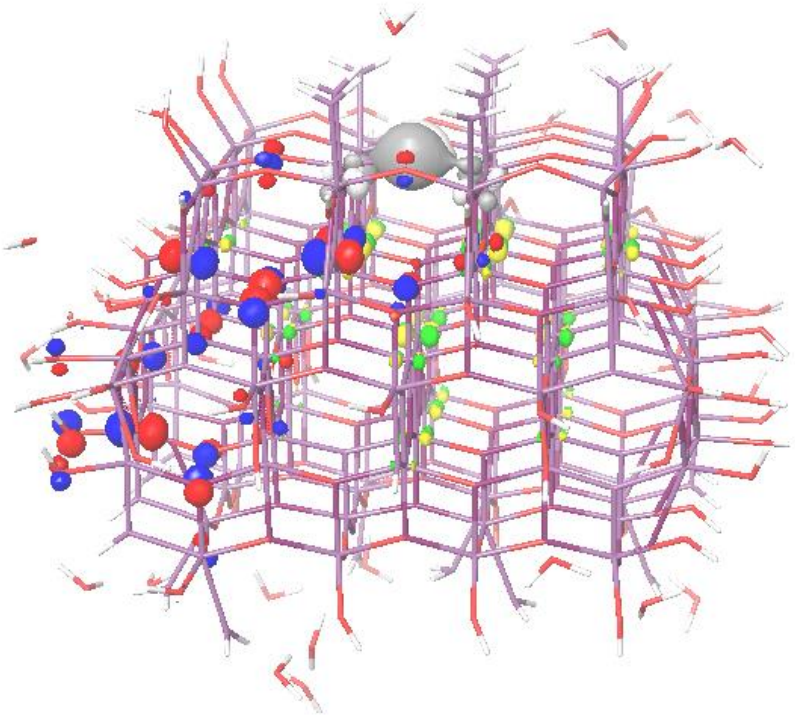

Figure 10 - Visualization of the hole (gray and white orbital) localized on a O_{2c} surface atom at the beginning of pulling experiment of the large cationic nanoparticle. The character and location of the hole is unchanged from the start of the pulling experiment. The LUMO and HOMO are also visualized in green and yellow, and blue and red, respectively.

Further, the charge on the reconstructing O atom where the hole localized does not change over the course of the pulling experiments. At the same time, the transferring electron moves from the adsorbate to nowhere near that atom in both neutral and cationic pulling systems: the surface Ti atom bears the most amount of its density (in edge cases, the e^- density is shared more evenly among the Ti atoms defining the edge ring. See Appendix A.3.1). We chose to study the PCET at the adsorbed waters that we did by their physical proximity to the hole; we see no reason why any other choices would more likely result in the hole being filled.

In fact, we find it should come as no surprise that the e^- does not fill the hole in the cationic pulling experiments: from the start of the experiments the orbital energy of the hole is well within the HOMO-LUMO gap, closer to the LUMO, and it remains there throughout the

entirety of the experiments. From the density of states plot in Fig. 14 (Appendix A.2.1), it should not be expected that the electron fills the hole in the cationic pulling experiment. Without an additional source of energy, there was never any way even the HOMO e^- — let alone the transferring e^- — would have enough energy to reach the hole orbital, whose oxidizing power in the relaxed cationic nanoparticle is far too low for that to occur.

However, we have found that role #2 of the hole is indeed filled: it was shown in Section 4.3.1 that the overpotential for the medium cationic nanoparticle, in which holes are present, is lower than that for the neutral nanoparticle by almost 0.2 eV. Rather than the reason being that the hole assists the electron transfer, making it concerted with the PT and lowering the overall energy, our results suggest that the hole likely aids the PCET by reducing the amount of negative charge nearby the H_3O^+ available to electrostatically resist its diffusion away from the nanoparticle surface. This is so because the O_{2p} orbital that the hole localizes in is simply too high energy for an e^- to occupy, effectively blocking out some degree of negative charge from the local region.

Regardless of why or that the total overpotential is smaller when there are holes present, it is still a major problem for the overall, longer-term functioning of the cell that the holes are not annihilated by the transferring electrons (role #1). Even if the cell were to run well for a few cationizations, the building up of holes at the surface would degrade the electronic and physical structures of the nanoparticle too much to function long. We can therefore draw one of two conclusions from our results: (1) that our model of the system is insufficient for addressing the capture of the transferring e^- by the hole, or (2) that what we find is faithful to experiment — that role #1 is not a function of the hole — and we must therefore resolve the presence of the

hole helping the PCET to occur but in a way different than directly filling the holes generated, which doesn't occur.

4.3.4 Resolving the Presence of the Hole

If indeed the hole is not annihilated by the transferring e^- during the first PCET of the OER on anatase TiO_2 nanoparticles, we must consider the effects of the continued presence of the hole after completion of the PCET. First, it is possible that the hole gets annihilated at another time during the OER and that the remaining steps of the OER shown in eq. 5 are not actually what occurs in experiment. Or, perhaps an additional step must be added in which an additional photoexcitation by a photon of lower energy fills the hole and resets the electronic structure of the system.

Otherwise, if the hole really does not get annihilated during the OER (in which case possibly three more holes would be created during the rest of the OER), it is possible that the kinetic overpotential suggested in this study is not the true cause of the high overpotential and that instead it is the build-up of holes. However, we find this unlikely, as it would result in an overpotential of at least 2.82 eV in the medium nanoparticle and 2.73 eV in the large one (i.e. the difference in energy between the HOMO and the hole), which is not in agreement with previous experiments and computational studies showing drastically lower overpotentials; instead, the overpotential obtained in this study results in overpotentials in much better alignment with prior studies, as indicated in Section 4.3.1.

Even if the presence of the hole is not the cause of the overpotential, its negative consequences, such as those discussed at the start of Section 4.3.3, may be the reason that TiO_2, while the prototypical anodic material and that used in the original Fujishima-Honda water

splitting experiment in 1972, is not a good catalyst from a practical standpoint and is why other materials are more often used in practice. It is plausible that other materials, when simulated using the methodology of this work, would result in a hole with low enough energy to be filled by an electron in the valence band.

We propose one modification to our system for creating such a material: p-doping the anatase TiO_2 by replacing some of the O atoms with N atoms, which seek an oxidation state of -3 in order to achieve noble gas valence. If the hole were localized on one of the N atoms — which would have an oxidation state of roughly -1.5 after forming two covalent bonds with Ti atoms and hosting the hole — near the PCET site, then upon the PT the transferring e^- would perhaps be pulled more strongly to the N atom, helping to annihilate the hole in the case that the transferring e^- indeed ended up localized on the N atom. While this may simply fill the acceptor state introduced by the N atom dopant, the fact that the e^- would be present on the same atom at which the hole was localized may somehow aid in filling the hole itself, particularly if the photoexcited nanoparticle had not yet completely relaxed, as explained in the next section.

4.3.5 Improvements for Describing Capture of the Transferring Electron by the Hole

If our model is insufficient for describing the e^- capture by the hole, we envision a few ways to improve it for this purpose. First, rather than using a fully relaxed cationic nanoparticle for the pulling experiments, we could use a nanoparticle that is not fully relaxed. After an e^- is kicked off the neutral nanoparticle, the LUMO energy (i.e., that of the just-vacated orbital) is very nearly the same as that of the neutral HOMO, as expected since cationization of the nanoparticle in Jaguar simply removes the highest-energy e^- from the system. As the

nanoparticle relaxes, the LUMO energy increases well into the band gap. Thus, using an incompletely optimized cationic nanoparticle would make the hole more energetically accessible to the transferring e^-.

A second way to improve the model so that the hole captures the transferring e^- is to account for multiple photoexcitations; it has been shown [19] that the higher the intensity of the incident light, the stronger the oxidizing power of the hole. Third, it has been found that the photoexcited e^- comes from an orbital within the bulk of the nanoparticle rather than on the surface, generally resulting in a much lower-energy photoexcited hole, whose orbital energy increases as it gradually diffuses to the surface. While hole diffusion is interesting on its own, if this were accurately modeled, the oxidation power of the hole may again be strong enough for valence electrons to fall in energy into its orbital, at least before the hole makes it all the way to the surface.

We note that even though these approaches may produce holes with enough oxidizing power to be filled by the transferring e^-, they may instead produce holes higher in energy than that of the transferring e^-, just as the method used in this work. In these cases, finite temperature calculations or excited state calculations might be employed in order for the hole to be filled by the transferring e^-.

If in experiment the photoexcited holes are indeed filled by the transferring electrons and our current model is therefore insufficient to describe this process, we stress that the inadequacies of the model may be limited to this particular effect. Our model and methodology are still the most comprehensive we have seen in literature for studying these types of phenomena [12] and the rest of our findings should still serve as a good first-order

approximation to more advanced studies, the results of which could be resolved with this work in order to make sense of the improvements they afford.

Chapter 5: Conclusion

While we performed several pulling experiments on the medium nanoparticle, we performed a single pulling experiment on the large nanoparticle due to its large system size requiring demanding computational resources. We chose this balance for two main reasons. First, it was important to run any calculations at all on the large nanoparticle in order to verify the properties found for the cationic version of the medium nanoparticle, in particular, the localization of the hole on a surface O3c atom. By running the optimization on the cationic version of the large nanoparticle and finding localization of the hole instead on an O_{2c} atom, we were able to determine that this particular finding for the medium nanoparticle was not generalizable to larger systems.

Second, if the medium nanoparticle was not ostensibly representative of the large nanoparticle, could the results of the pulling experiments on the medium nanoparticle still be trusted to apply to larger systems? For example, would the hole in the large nanoparticle annihilate the transferring e^-? We find that the qualitative and quantitative results of the medium cationic pulling experiment on the large nanoparticle are similar to those on the medium nanoparticle. For example, just as in the medium nanoparticle, the charge on the O_{2c} atom housing the hole remains at $-0.55e$ to $-0.53e$ throughout the entire pulling experiment, suggesting that the hole may indeed generally have nothing to do with the ET. Thus, overall, we find no reason to doubt that any of our findings for the medium nanoparticle hold too for the large nanoparticle — which is the same order of magnitude in size as realistic anatase TiO_2 nanoparticles [28, 61] — and we conclude that it may not be necessary to run the other pulling experiments on the large nanoparticle pulling from a different adsorbate water molecule, saving

significant computing resources, and instead extrapolating the results from those from the medium nanoparticle.

A major finding of this study was the role that the hole plays in the first PCET and what that means for the overpotential associated with the process. Identifying the source of the overpotential would very useful in designing and engineering a way around the problem, however that isn't tractable without knowing the nature of the inefficiency. We have found that the source of the overpotential of the first PCET mostly comes from the instability of the species generated at the end of the PCET – namely, the adsorbate *OH. Although there is a transition state peak on the total system energy vs. reaction coordinate curves (correlating to the region where the newly-formed hydronium ion diffuses away from the system), this region is not much higher in energy than the product state plateau itself. The difference in total energy between the react and product states was 1.08 eV and 1.09 eV for the medium and large cationic nanoparticles, with the kinetic contribution (peak height relative to product state) amounting only to an additional 0.25 eV and 0.45 eV, respectively. Thus, we see that most of the increase in energy comes from the formation of the *OH adsorbate, with a smaller, additional penalty to have the hydronium diffuse away. We underscore that it is important to include the diffusion of the hydronium ion away from the nanoparticle after the proton transfer to it takes place – not just the transfer of the proton from the adsorbate O atom to the target water's O atom – in order to capture the true transition state of the PCET.

The hole itself does not appear to play a direct role in the PCET – as mentioned in Section 4.3.3, the hole localizes on a surface O_{2c} atom as soon as the nanoparticle is made cationic, remains there throughout the course of the optimizations and pulling experiments, and the properties of the hole remain constant. This remains true regardless of system size and where we

abstract the PCET proton from: it is perhaps the feature that is the most remarkably invariant over all of our different experiments. The hole is not filled by the electron transferring in the PCET, or any other atom – it persists at too high of an energy for that to occur.

While the presence of the hole does reduce the amount of energy required for the PCET, it isn't because it aids the electron transfer from the adsorbate water into the nanoparticle: we don't find that that happens. Instead, we posit that the hole blocks out electron density from the surface of the nanoparticle near the hydronium ion diffusing away, thereby avoiding a situation where that electron density would otherwise electrostatically resist and hinder that from happening.

While we focused on the first PCET of the OER in this study, we can use what we learned to hypothesize about the rest of the OER. We posit that the major factor in determining the energy required for the OER is the type of bond the intermediate species has with the surface Ti atom at the beginning of each PCET, verifying what others have found [64, 68], and that this bond type is dependent not on the stage of the OER but instead only on which surface is being studied. This is a direct consequence of the coordination structure of the surface Ti atom. For example, as we found that a Ti atom in the anatase TiO_2 bulk tends to strongly donate an electron to each of four covalent bonds separated by about 90° about its equator, throughout the OER on the (001) surface the Ti atom will have always "used up" its four covalent bonds so that the two bonds at its poles, including that with the surface species, must be donor-acceptor in nature. Further, as we found this bond prior to the first PCET to be weak and the "direction" of the negative charge to be from the adsorbate O atom to the surface Ti, we suspect that this bond will be of the same nature prior to the other three PCETs. Similarly, throughout the OER on the (101) surface the "orientation" of the coordination structure of the surface Ti atom will be constant so

that the bond with the surface species throughout the OER will be covalent, with the Ti atom donating negative charge strongly to the adsorbate O atom.

We posit that the mechanism proposed my Nakamura et al. [16] is not likely. It requires that the OER is started by the direct attack of a water molecule attacking a surface lattice O_{2c} atom, which our findings don't support; the hole appears to play no direct role in the OER, or at least the rate-determining first PCET. We find the PCET proceeds via a nucleophilic attack by a water on an undercoordinated Ti_{5c} atom on the surface, adjacent to the hole O atom. The hole localizes on and remains trapped at this surface lattice O_{2c} site and, as the proton is transferred away from the nanoparticle, the displaced electron density resides rather delocalized on the nanoparticle, too low in energy to fill the hole.

Looking toward future work, it may be interesting to, rather than using ground-state DFT on a neutral nanoparticle, we could try the simulations using time-dependent DFT (TDDFT) on a neutral nanoparticle. This may be a more realistic way to model the system anyway, as in the real system there may be H^+/H_3O^+ species near the surface of the nanoparticle that induce the formation of trap states for the photoexcited electrons. This, most importantly, may also produce a more accessible photoexcited hole in the valence band of the nanoparticle, although if the nanoparticle were fully optimized using TDDFT and the hole did not interact with the e^-, then it is likely the hole would again increase in energy into the band gap like we say as it relaxes to the surface. In this case, the qualitative results from using DFT on the ground-state cationic nanoparticle and TDDFT on the neutral nanoparticle would approximate each other. We note that using TDDFT the hole would be more accessible (at least before optimization) if the excitation occurs from a non-HOMO orbital, one of lower energy, so that the effective Fermi level of the hole would be below the valence band edge, allowing it to be filled by an electron

from a higher-energy orbital. That being said, hole relaxation to the top of the valence band is several orders of magnitude quicker than the subsequent chemical reaction occurring at the surface, so ground-state DFT seems reasonable to describe the hole trapped at the surface accurately [59, 69]. Moreover, the use of TDDFT and how it performs in the description of relaxation processes (i.e. the time evolution of large systems starting from a nonequilibrium condition) is largely unknown and untested [70, 71]. Treating our system using TDDFT and comparing those results to those obtained here with ground-state DFT on the cationic nanoparticles could help elucidate how TDDFT performs in these systems.

Additionally, it would be valuable to see how the second PCET of the OER proceeds by doing a second cationization of our large nanoparticle and subsequent second pulling experiment. Where would the second hole localize on our system? Would holes continue to collect on the surface of the nanoparticle on bridging oxygen sites for subsequent cationizations? We saw in our large cationic nanoparticle system that the lengths of the bonds of the hole-localized O atom to the Ti atom on either side of it noticeably lengthen due to the presence of the hole. It is possible that a second hole localized on this O atom could break a bond to one of the Ti atoms, liberating that surface O atom to potentially directly participate in the OER and/or provide a way for the holes to fill up and for the surface to "heal" itself of the holes. Experimentalists studying catalytic water splitting in TiO_2 indeed find isotopic evidence that surface lattice O atoms are liberated from the surface to participate in the OER and evolve as part of an oxygen molecule generated in the end [72]. Solvent water molecules adsorb at the resulting oxygen vacancies, healing the nanoparticle's structure. Studying the subsequent PCETs of the OER could reveal if this mechanism is plausible [73].

Additionally, it would be interesting to continue simulating proceeding PCETs with our pulling experiments to study the overpotentials associated with them in their own right. Experimentalists have found [3, 15, 67, 74] a linear relationship between bond strengths of three water-derived intermediates that are generated over the course of the OER regardless of catalytic surface: *OH, *O, and *OOH. Namely, they show that the free energy of the second and third reaction steps sum to a constant amount of 3.2 eV on both metals and oxide surfaces, regardless of binding site and of *O intermediate binding strength. Put another way, $\Delta G_2 + \Delta G_3 = 3.2$ eV across all metal and metal oxide surfaces. An ideal water-splitting catalyst would split this difference evenly, adsorbing just strongly enough that the binding strength of the *O intermediate places the free energy of the associated reaction step 1.6 eV from that of either *OH or *OOH. When the binding of *O to the surface is stronger, ΔG_2 grows and when the binding of it is weaker, ΔG_3 grows; depending on its binding strength, the second or third PCETs may become sufficiently large to be potential-determining. However, even split evenly down the middle, there would appear to be an effectively unavoidable overpotential of at least about 0.37 eV, since the lowest-possible potential 1.6 eV is 0.37 eV above the 1.23 eV theoretically required. It is proposed that the invariance in binding strength between *OH and *OOH comes from the similar nature of the bonds (oxygen atom single bonded to an undercoordinated metal atom; the *O intermediate involves a double bond and is hence naturally different). Surface modifications, like doping the surface of a TiO_2 nanoparticle with other metals in order to tune the bonding strength to a level that places the *O intermediate ideally halfway between the 3.2eV gap between *OH and *OOH intermediates, should optimize OER efficiency. Metals deposited on TiO_2 represent other, alternative complexes studied to help optimize OER catalytic activity, and while they do reduce the band gap of the material, electrons tend to accumulate at the

epitaxial surface [75]. However, it is important to note that these modifications come with trade-offs of their own, like necessitating the use of expensive, unabundant, and/or toxic dopant metals or co-catalysts. Additionally, honing operating conditions (e.g. pH level) to help tune the binding strength to the ideal level is also possible, though other consequences (like deterioration of the integrity of the nanoparticles) need to be considered at the same time.

References

[1] A. S. Barnard, P. Zapol, L. A. Curtiss. Modeling the Morphology and Phase Stability of TiO2 Nanocrystals in Water. *Journal of Chemical Theory and Computation*, 1(1):107—116, 2005.

[2] A. J. Nozik. Photoelectrolysis of water using semiconducting TiO2 crystals. *Nature*, 257(5525):383—386, 1975.

[3] Isabela C. Man, Hai-Yan Su, Federico Calle-Vallejo, Heine A. Hanson, Jose. I. Martínez, Nilay G. Inoglu, John Kitchin, Thomas F. Jaramillo, Jens K. Nørskov, and Jan Rossmiesl. Universality in Oxygen Evolution Electrocatalysis on Oxide Surfaces. *ChemCatChem*, 3(7):1159-1165, July 2011.

[4] Marie-Isabelle Baraton. Nano-TiO_2 for Solar Cells and Photocatalytic Water Splitting: Scientific and Technological Challenges for Commercialization. *The Open Nanoscience Journal*, 5:64-77, 2011.

[5] Marc T. M. Koper. Theory of Multiple Proton–Electron Transfer Reactions and its Implications for Electrocatalysis. *Chem. Sci.*, 4(7):2710-2723, February 2013.

[6] Tim Luttrell, Sandamali Halpegamage, Junguang Tao, Alan Kramer, Eli Sutter, and Matthias Batzill. Why is anatase a better photocatalyst than rutile? – Model studies on epitaxial TiO2 films*. Scientific Reports,* 4:4043, February 2014.

[7] M. Xu, Y. Gao, E.M. Moreno, M. Kunst, M. Muhler, Y. Wang, and C. Wöll. Photocatalytic activity of bulk TiO2 anatase and rutile single crystals using infrared adsorption spectroscopy. *Physical Review Letters,* 106(13):138302. March 2011.

[8] L.K. Preethi, T. Mathews, M. Nand, S.N. Jha, C.S. Gopinath, and S. Dash. Band alignment and charge transfer pathway in three phase anatase-rutile-brookite TiO2 nanotubes: An efficient photocatalyst for water splitting. *Applied Catalysis B: Environmental*, 218:9-19, December 2017.

[9] Gonghu Li and Kimberly A. Grey. The solid-solid interface: Explaining the high and unique photocatalytic activity of TiO2-based nanocomposite materials. *Chemical Physics,* 339(1-3):173-187, October 2007.

[10] Mingchun Xu, Youkun Gao, Elias Martinez Moreno, Marinus Kunst, Martin Muhler, Yuemin Wang, Hicham Idriss, and Christof Wöll. Photocatalytic Activity of Bulk TiO2 Anatase and Rutile Single Crystals Using Infrared Absorption Spectroscopy. *Physical Review Letters*, 106(13):138302, March 2011.

[11] Benjamin Klahr, Sixto Jiminez, Francisco Fabregat-Santiago, Juan Bisquert, and Thomas W. Hamann. Photoelectrochemical and Impedance Spectroscopic Investigation of Water Oxidation with “Co–Pi”–Coated Hematite Electrodes. *J. Am. Chem. Soc.*, 134(40):16693-16700. September 2012.

[12] Yeliz Gurdal and Marcella Iannuzzi. DFT-based Theoretical Simulations for Photocatalytic Applications Using TiO2. *Titanium Dioxide*, July 2017. DOI: 10.5772/intechopen.68979.

[13] Muhammed Nur Iman Amir, Nurhidayatullaili Muhd Julkapli, Samira Bagheri, and Amin Termeh Yousefi. TiO_2 Hybrid Photocatalytic Systems: Impact of Adsorption and Photocatalytic Performance. *Reviews in Inorganic Chemistry*, 35(3):151-178, August 2015.

[14] Ye-Fei Li, Zhi-Pan Liu, LuLu Liu, Weiguo Gao. Mechanism and Activity of Photocatalytic Oxygen Evolution on Titania Anatase in Aqueous Surroundings. *J. Am. Chem. Soc.*, 132(37):13008—13015, 2010.

[15] Vincent C.-C. Wang. Exploring the Kinetic and Thermodynamic Aspects of Four-Electron Electrochemical Reactions: Electrocatalysis of Oxygen Evolution by Metal Oxides and Biological Systems. *Phys. Chem. Chem. Phys.*, 18(32):22364-22372, July 2016.

[16] R. Nakamura and Y. Nakato. Primary Intermediates of Oxygen Photoevolution Reaction on TiO2 (Rutile) Particles, Revealed by in Situ FTIR Adsorption and Photoluminescence Measurements. *J. Am. Chem. Soc.*, 126(4):1290-1298, 2004.

[17] Jun Cheng, Xiandong Liu, John A. Kattirtzi, Joost VandeVondele, and Michiel Sprik. Aligning Electronic and Protonic Energy Levels of Proton-Coupled Electron Transfer

in Water Oxidation on Aqueous TiO_2. *Angew. Chem. Int. Ed.*, 53(45):12046-12050, November 2014.

[18] Shizhong Liu, Michael G. White, and Ping Liu. Mechanism of Oxygen Reduction Reaction on Pt(111) in Alkaline Solution: Importance of Chemisorbed Water on Surface. *J. Phys. Chem. C*, 120(28):15288-15298, June 2016.

[19] Á. Valdés, Z.-W. Qu, G.-J. Kroes, J. Rossmeisl, J. K. Nørskov. Oxidation and Photo-Oxidation of Water on TiO2 Surface. *The Journal of Physical Chemistry C*, 112(26):9872—9879, 2008.

[20] Oberhofer, H. In Handbook of Materials Modeling: Applications: Current and Emerging Materials; Andreoni, W., Yip, S., Eds.; Springer International Publishing: Cham, 2018:1–33. DOI: https://doi.org/10.1007/978-3-319-50257-1

[21] Michael G. Walter, Emily L. Warren, James R. McKone, Shannon W. Boettcher, Qixi Mi, Elizabeth A. Santori, and Nathan S. Lewis. Solar Water Splitting Cells. *Chem. Rev.*, 110(10):6446-6473, November 2010.

[22] N.Z. Muradov, T.N. Veziroğlu. *Int. J. Hydrogen Energy*, 33(23): 6804-6839, December 2018.

[23] Milana Trifkovik, Mehdi Sheikhzaded, Khaled Nigim, and Prodromos Daoutidis. Modeling and Control of a Renewable Hybrid Energy System With Hydrogen Storage. *IEEE Transactions on Control Systems Technology*, 22(1):169-179, January 2014.

[24] M. S. Dresselhaus and I. L. Thomas. Alternative Energy Technologies. *Nature*, 414:332-337, November 2001.

[25] A. Fujishima and K. Honda. Electrochemical Photolysis of Water at a Semiconductor Electrode. *Nature*, 238(5358):37-38, 1972.

[26] G. Sivalingam, K. Nagaveni, M.S.. Hegde, and G. Madras. Photocatalytic degradation of various dyes by combustion synthesized nano anatase TiO2. *Applied Catalysis B: Environmental*, 45(1):23-28, September 2003.

[27] Moussab Harb, Gabriel Jeantelot, and Jean-Marie Basset. Insights into the Most Suitable TiO_2 Surfaces for Photocatalytic O_2 and H_2 Evolution Reactions from DFT Calculations. *J. Phys. Chem. C*, 123(46): 28210-28218, October 29, 2019.

[28] H. Tang, K. Prasad, R. Sanjinès, P.E. Schmid, and F Lévy. Electrical and optical properties of TiO2 anatase thin films. *Journal of Applied Physics*, 75(4):2042, 1994.

[29] Anqi Wang, Kang Hu, Yuqian Liu, Ruiqi Li, Chenlu Ye, Zixiao Yi, Kai Yan. Flower-like MoS_2 with Stepped Edge Structure Efficient for Electrocatalysis of Hydrogen and Oxygen Evolution. *Int. J. Hydrog. Energy*, 44(13):6573-6581, March 2019.

[30] Douglas R. Kauffman, Xingyi Deng, Dan C. Sorescu, Thuy-Duong Nguyen-Phan, Congjun Wang, Chris M. Marin, Eli Stavitski, Iradwikanari Waluyo, and Adrian Hunt. Edge-Enhanced Oxygen Evolution Reactivity at Ultrathin, Au-Supported Fe_2O_3 Electrocatalysts. *ACS Catal.*, 9(6):5375-5382, May 2019.

[31] Wen Qi Fang, Xue-Qing Gong, Hua Gui Yang. On the Unusual Properties of Anatase TiO2 Exposed by Highly Reactive Facets. *The Journal of Physical Chemistry Letters*, 2(7)725-734, April 2011.

[32] Filippo De Angelis, Cristiana Di Valentin, Simona Fantacci, Andrea Vittadini, Annabella Selloni. Theoretical Studies on Anatase and Less Common TiO2 Phases: Bulk, Surfaces, and Nanomaterials. *Chemical Reviews*, 2014.

[33] Amy L. Linsebigler, Guangquan Lu, and John T. Yates. Photocatalysis on TiO_2 Surfaces: Principles, Mechanisms, and Selected Results. *Chem. Rev.*, 95(3):735-758, May 1995.

[34] Thomas R. Gordon, Matteo Cargnello, Taejong Paik, Filippo Mangolini, Ralph T. Weber, Paolo Fornasiero, and Christopher B. Murray. Nonaqueous Synthesis of TiO2 Nanocrystals Using TiF4 to Engineer Morphology, Oxygen Vacancy Concentration, and Photocatalytic Activity. *Journal of the American Chemical Society*, 134(15):6751-6761, April 2012.

[35] D. Lawless, N. Serpone, and D. Meisel. Role of hydroxyl radicals and trapped holes in photocatalysis. A pulse radiolysis study. *J. Phys. Chem.*, 95(13):5166-5170, June 1991.

[36] Jing Zhang, Thomas F. Hughes, Michael Steigerwald, Louis Brus, and Richard A. Friesner. Realistic Cluster Modeling of Electron Transport and Trapping in Solvated TiO2 Nanoparticles. *J. Am. Chem. Soc.*, 134(29):12028-12042, July 2012.

[37] Marcella Iannuzzi and Jürg Hutter. Comparative Study of the Nature of Chemical Bonding of Corrugated Graphene on Ru(0001) and Rh(111) by Electronic Structure Calculations. *Surface Science*, 605(15-16):1360-1368, August 2011.

[38] M. Verónica Ganduglia-Pirovano, Juarez L. F. Da Silva, and Joachim Sauer. Density-Functional Calculations of the Structure of Near-Surface Oxygen Vacancies and Electron Localization on CeO_2(111). *Phys. Rev. Lett.*, 102(2):026101, January 2009.

[39] J. C. Slater. A simplification of the Hartree-Fock Method. *Phys. Rev.*, 81(3):385-390, February 1951.

[40] Claudius Kormann, Detlef W. Bahnemann, and Michael R. Hoffmann. Preparation and Characterization of Quantum-Sized Titanium Dioxide. *J. Phys. Chem.*, 92(18):5196-5201, September 1988.

[41] F.H. Allen, G. Bergerhoff, and I.D. Brown. In *Crystallographic Databases* . International Union of Crystallography, 1987.

[42] R. Antony, T. Mathews, C, Ramesh, N. Murugesan, A. Dasgupta, S. Dhara, S. Dash, and A.K. Tyagi. Efficient photocatalytic hydrogen generation by Pt modified TiO2 nanotubes fabricated by rapid breakdown anodization. *International Journal of Hydrogen Energy*, 37(10):8268-8276, May 2012.

[43] Ye-Fei Li and Annabella Selloni. Pathway of Photocatalytic Oxygen Evolution on Aqueous TiO_2 Anatase and Insights into the Different Activities of Anatase and Rutile. *ACS Catal.*, 6(7):4769-4774, June 2016.

[44] Jiajie Fan, Weiquan Cai, and Jiaguo Yu. Adsorption of N719 Dye on Antase TiO2 Nanoparticles and Nanosheets with Exposed (001) Facets: Equilibrium, Kinetic, and Thermodynamic Studies. *Chemistry – An Asian Journal*. 6(9):2481-2490, September 2011.

[45] Mi-Hee Jung, Moo-Jung Chu, and Ma Gu Kang. TiO2 nanotube fabrication with highly exposed (001) facets for enhanced conversion efficiency of solar cells. 48(10):5016-5018, April 2012.

[46] Jianwei Miao and Bin Liu. Anatase TiO2 microspheres with reactive {001} facets for improved photocatalytic activity. *RSC Advances*, 3(4):1222-1226, December 2012.

[47] Weiguang Yang, Jianming Li, Yali Wang, Feng Zhu, Weimin Shi, Farong Wan, and Dongsheng Xu. A facile synthesis of anatase TiO2 nanosheets-based hierarchical spheres with over 90% {001} facets for dye-sensitized solar cells. 47)6):1809-1811, January 2011.

[48] Jiaguo Yu, Jiajie Fan, and Kangle Le. Anatase TiO2 nanosheets with exposed (001) facets: improved photoelectric conversion efficiency in dye-sensitized solar cells. 2(1):2144-2149, October 2010.

[49] Yiwei Hu, Tao Ding, Kailong Zhang, Biao Li, Baichuan Zhu, and Kaibin Tang. Component-Tunable Rutile-Anatase TiO_2/Reduced Graphene Oxide Nanocomposites for Enhancement of Electrocatalytic Oxygen Evolution. *ChemNanoMat*, 4(11):1133-1139, November 2018.

[50] A. Vittadini, A. Selloni, F. P. Rotzinger, and M. Grätzel. Structure and Energetics of Water Adsorbed at TiO_2 Antaise (101) and (001) Surfaces. *Phys. Rev. Lett*., 81(14):2954-2957, October 1998.

[51] Binghui Wu, Changyou Guo, Nanfeng Zheng, Zhaoxiong Xie, and Galen D. Stucky. Nonaqueous Production of Nanostructured Anatase with High-Energy Facets. *J. Am. Chem. Soc.*, 130(51):17563-17567, November 2008.

[52] Jian Pan, Gang Liu, Gao Qing (Max) Lu, and Hui-Ming Cheng. On the True Photoactivity Order of {001}, {010}, and {101} Facets of Anatase TiO2 Crystals. *Angewandte Chemie International Edition*, 50(9):2133-2137, February 2011.

[53] Aaron Wold. Photocatalytic Properties of Titanium Dioxide (TiO_2). *Chem. Mater.*, 5(3):280-283, March 1993.

[54] Ke Fang, Guanxing Li, Yang Ou, Wentao Yuan, Hangsheng Yang, Ze Zhang, Yong Wang. An Environmental Transmission Electron Microscopy Study of the Stability of the TiO_2 (1 × 4) Reconstructed (001) Surface. *The Journal of Physical Chemistry C*, 123(35):21522-21527, August 2019.

[55] Wilhelm Hebenstreit, Nancy Ruzycki, Gregory S. Herman, Yufei Gao, Ulrike Diebold. Scanning tunneling microscopy investigation of the TiO2 anatase (101) surface. *Phys. Rev. B*, 62(24):R16334—R16336, 2000.

[56] Jing Zhang, Andrew L. Weisman, Patrick Saitta, Richard A. Friesner. Efficient Simulation of Large Materials Clusters Using the Jaguar Quantum Chemistry Program: Parallelization and Wavefunction Initialization. *International Journal of Quantum Chemistry*, 116(5):357-368, March 2016.

[57] Ulrike Diebold. Growth, surface characterization, and reactivity of TiO2 anatase films - EPSCOR. 2004.

[58] Patrick Gono, Francesco Ambrosio, and Alfredo Pasquarello. Effect of the Solvent on the Oxygen Evolution Reaction at the TiO_2–Water Interface. *J. Phys. Chem. C*, 123(30):18467-18474, July 2019.

[59] Jia Chen, Ye-Fei Li, Patrick Sit, Annabella Selloni. Chemical Dynamics of the First Proton-Coupled Electron Transfer of Water Oxidation on TiO2 Anatase. *J. Am. Chem. Soc.*, 135(50):18774—18777, 2013.

[60] Laurence M. Peter. Photoelectrochemical Water Splitting. A Status Assessment. *Electroanalysis*, 27(4):864—871, 2015.

[61] Mabrook S. Amer, Mohamed A. Ghanem, Prabhakarn Arunachalam, Abdullah M. Al-Mayouf, and Talal A. Aljohani. Modification of Mesoporous Titanium Dioxide with Cobalt Oxide Electrocatalyst for Enhanced Oxygen Evolution Reaction. *Advanced Materials Letters*, 10(2):136-144, February 2019.

[62] Bin Liu, Mao Ming Chen, Chong Liu, Sean C. Andrews, Chris Hahn, and Peidong Yang. Large-Scale Synthesis of Transition-Metal-Doped TiO_2 Nanowires with Controllable Overpotential. *J. Am. Chem. Soc.*, 135(27):9995-9998, July 2013.

[63] Joaquin Resasco, Neil P. Dasgupta, Josep Roque Rosell, Jinghua Guo, and Peidong Yang. Uniform Doping of Metal Oxide Nanowires Using Solid State Diffusion. *J. Am. Chem. Soc.*, 136(29):10521-10526, July 2014.

[64] J. Rossmeisl, Z.-W. Qu, H. Zhu, G.-J. Kroes, J.K. Nørskov. Electrolysis of Water on Oxide Surfaces. *Journal of Electroanalytical Chemistry*, 607(1-2):83-89, September 2007.

[65] F. Rodriguez-Hernández, D.C. Tranca, A. Martínez, Ll Uranga-Piña, and G. Seifert. Water Splitting on Transition Metal Active Sites at TiO_2-Based Electrodes: A small Cluster Study. *J. Phys. Chem. C*, 120(45):25851-25860, October 2016.

[66] Charles C. L. McCrory, Suho Jung, Jonas C. Peters, Thomas F. Jaramillo. Benchmarking Heterogeneous Electrocatalysts for the Oxygen Evolution Reaction. *J. Am. Chem. Soc.*, 135(45): 16977-16987, October 2013.

[67] Hua Bing Tao, Liwen Fang, Jiazang Chen, Hong Bin Yang, Jiajian Miao, Chengli Chen, and Bin Liu. Identification of Surface Reactivity Descriptor for Transition Metal Oxides in Oxygen Evolution Reaction. *J. Am. Chem. Soc.*, 138(31):9978-9985, July 2016.

[68] J. Rossmeisl, A. Logadottir, and J.K. Nørskov. Electrolysis of Water on (oxidized) Metal Surfaces. *Chemical Physics*, 319(1-3):178-184, December 2005.

[69] Alexander J. Cowan, Christopher J. Barnett, Stephanie R. Pendlebury, Monica Barroso, Kevin Sivula, Michael Grätzel, James R. Durrant, David R. Klug. Activation Energies for the Rate-Limiting Step in Water Photooxidation by Nanostructured α-Fe2O3 and TiO2. *Journal of the American Chemical Society*, 133(26):10134—10140, 2011.

[70] Kieron Burke, Jan Werschnik, and E. K. U. Gross. Time-dependent Density Functional Theory: Past, Present, and Future. *J. Chem. Phys.*, 123:062206, August 2005.

[71] K. Burke, R. Car, and R. Gebauer. Density Functional Theory of the Electrical Conductivity of Molecular Devices. *Phys. Rev. Lett.*, 94(14):146803, April 2005.

[72] J.F. Montoya, D. W. Bahnermann, P. Salvador, and J. Peral. Catalytic Role of Bridging Oxygens in TiO_2 Liquid Phase Photocatalytic Reactions: Analysis of $H_2{}^{16}O$ Photooxidation on Labeled $Ti^{18}O_2$. *Catal. Sci. Technol.*, 7(4):902-910, January 2017.

[73] Xueqing Zhang, Peter Klaver, Rutger van Santen, M.C.M. van de Sanden, and Anja Bieberle-Hütter. Oxygen Evolution at Hematite Surfaces: The Impact of Structure and Oxygen Vacancies on Lowering the Overpotential. *J. Phys. Chem. C*, 120(32):18201-18208, July 2016.

[74] Marc T. M. Koper. Thermodynamic Theory of Multi-Electron Transfer Reactions: Implications for Electrocatalysis. *J. Electroanal. Chem.*, 660(2):254-260, September 2011.

[75] Shi-Tong Zhang, Chang-Ming Li, Hong Yan, Min Wei, David G. Evans, and Xue Dwan. Density Functional Theory Study on the Metal-Support Interaction Between Ru Cluster and Anatase TiO_2(101) Surface. *J. Phys. Chem. C*, 118(7);3514-3522, January 2014.

[76] Alexander J. Cowan and James R. Durrant. Long-lived Charge Separated States in Nanostructured Semiconductor Photoelectrodes for the Production of Solar Fuels. *Chem. Soc. Rev.*, 42(6):2281-2293, September 2012.

Appendix: Supporting Information

A.1 Additional Simulation Methodology and Software Keywords

The normal keywords used in the &gen section for the TiO_2 nanoparticles studied for this paper are included below. The version of Jaguar used and to which these keywords apply is . Depending on the exact nanoparticle calculation, the keywords may have been slightly altered. For example, the molchg keyword and multip keyword were set to 0 and 1, respectively, for neutral nanoparticles, and were set to +1 and 0, respectively, for cationic nanoparticles. Unrestricted Hartree-Fock (iuhf = 1) was used for cationic systems only. Fields left blank mean the keyword was not explicitly included in the &gen section and so the default value was used.

The general methodology we employed to optimize a nanoparticle from start to finish is detailed here. From its MATLAB geometry (described in Section 3.1), we optimized the nanoparticle first with the Fragmented Initial Guess algorithm, employing corresponding keywords below. This was to generate a good enough initial guess for the system, as the guesses produced by Jaguar itself for transition-metal-containing clusters as large as those we studied would not converge. We then optimized the cluster with this initial guess in vacuum before optimizing it in solvent (water), as trying to go directly from FIG job to a solvent optimization would similarly not converge. Optimizing the cluster in vacuum allowed the cluster atoms to evolve (slightly) from their perfect anatase MATLAB geometry and provide a tractable guess, though we had to take care not to let the optimization go too far, as at a certain point the nanoparticle would begin to warp and the passivation begin to degrade. This guess was further refined with a properties calculation using the vacuum properties keywords, allowing the SCF calculation to converge over more iterations to achieve a more precise guess. The system was then optimized in water using the solvent opt keywords. Lastly, the system's guess was refined a

final time and several properties of its properties were printed out (frontier orbitals, charge populations of the atoms, etc.) using the solvent properties keywords below.

It should be pointed out that for the cationic clusters, no FIG or vacuum calculations were done - these were created by taking the corresponding neutral nanoparticle after the vacuum properties stage and starting a new solvent stage optimization with molchg set to +1 and multip set to 2. The initial guess for these systems were already good enough that such preliminary optimizations were unnecessary.

To summarize, the general strategy was to take the MATLAB geometry of a given TiO_2 nanoparticle and, first, get a good enough initial guess to start Jaguar calculations with, and then allow the nanoparticle to optimize a little bit (but not too much) in vacuum until we were able to optimize it in solvent water and obtain the relevant properties.

Keyword	FIG	Vac. Opt. Loose	Vacuum Opt.	Vacuum Properties	Solvent Opt.	Solvent Properties
allow_scf _failure	1	1	1	0	1	0
basis	lacvp	lacvp	lacvp	lacvp	lacvp	lacvp
cut20	2.00E-003	2.00E-003	2.00E-003	2.00E-003	2.00E-003	2.00E-003
dconv	3.00E-006	5.00E-006	3.00E-006	3.00E-006	3.00E-006	3.00E-006
dftname	B3LYP	B3LYP	B3LYP	B3LYP	B3LYP	B3LYP
econv	1.00E-005	5.00E-005	2.00E-005	1.00E-005	2.00E-005	1.00E-005
iacc	1					
iaccg		3	3	3	3	3
iacscf	4	4	4	4	4	4
igeopt	0	1	1	0	1	0
iguess	11	11	11	11	11	11
iorb1a		0	0	homo-1	0	homo-1
iorb2a		0	0	lumo+1	0	lumo+1
iorb1b		0	0	homo-1	0	homo-1
iorb2b		0	0	lumo+1	0	lumo+1
ipvirt		10	10	10	10	10
isolv		0	0	0	2	2
isymm	0	0	0	0	0	0
itradj	1	1	1	1	1	1
iuhf	0					
ldips		1	1	5	1	5
maxit	3	10	8	250	8	250
maxitg		10	300	1	300	1
molchg	0	0 or 1	0 or 1	0 or 1	0 or 1	0 or 1
mulken		0	0	1	0	1
multip		1 or 0	1 or 0	1 or 0	1 or 0	1 or 0
nofail	1					
nogas		2	2	2	2	2
nops	0	0	0	0	0	
solvent					water	water
tradmn		0.06	0.06	0.06	0.06	0.06
tradmx		0.2	0.2	0.2	0.2	0.2
trust		0.15	0.15	0.15	0.15	0.15

Table 7 - Keywords by calculation stage (&gen sections)

During the “pulling experiment” portion of this study, with the convergence of the large nanoparticle even more difficult to achieve than the medium nanoparticles given its larger size, special care was taken during its solvent optimization stage to ensure success. We froze all atoms more than 10 Å away from the target water oxygen atom to make the jobs computationally tractable, confident those atoms are too far away from the reaction site to be of consequence. Additionally, we allowed the step size the SCF calculation to start off larger than normal by increasing the tradmn, tradmx, and trust keywords. After it optimized for a while, we would stop the calculation, take the restart file with the current wavefunction, and restart the calculation with smaller step sizes (i.e. decreasing the value of the aforementioned keywords). We did this several times such that the last restart calculation for the solvent optimization stage was done using the normal values for tradmn, tradmx, and trust. One can think of the solvent optimization stage in this case as comprising four iterations, with decreasing step size. The values used for each step size are shown below.

Keyword	**Small Step**	**Medium 1 Step**	**Medium 2 Step**	**Large Step**
tradmn	0.06	0.06	0.06	0.06
tradmx	0.20	0.50	0.65	0.85
trust	0.15	0.45	0.60	0.80

Table 8 - Step size keywords

A.2 Detailed Geometry Optimization Results

A.2.1 Medium Nanoparticle

The geometries of the neutral (left) and cationic (right) versions of the optimized medium nanoparticle are shown in Fig. 11. The neutral version shows that the anatase structure is well-maintained, whereas the cationic version shows the surface reconstruction mentioned in Section 3.4. Fig. 12 shows the HOMO/LUMO/hole orbitals (top) and densities of state (bottom) of the neutral (left) and cationic (right) versions of the nanoparticle. The top-right subfigure shows that the hole resides on the "reconstructing" O atom, and the bottom-right subfigure shows the orbital energy of this hole to lie in the band gap, closer to the LUMO energy. It is confirmed from a Mulliken population analysis that the hole lies on this reconstructing O atom, with its charge increasing from $-0.90e$ in the neutral version to $-0.53e$ in the cationic version, compared to an average charge of $-0.92e$ on the other O_{3c} atoms and $-0.77e$ on the O_{2c} atoms on the top (001) surface of the cationic nanoparticle. The computed gap of the neutral nanoparticle is 4.62 eV and that of the cationic nanoparticle is 4.58 eV, excluding the hole state inside the gap, which is 3.12 eV above the HOMO and 1.46 eV below the LUMO. This is above the experimental value of 3.2 eV, however we expected our band gap to be overestimated as mentioned in the introduction in Section 3.

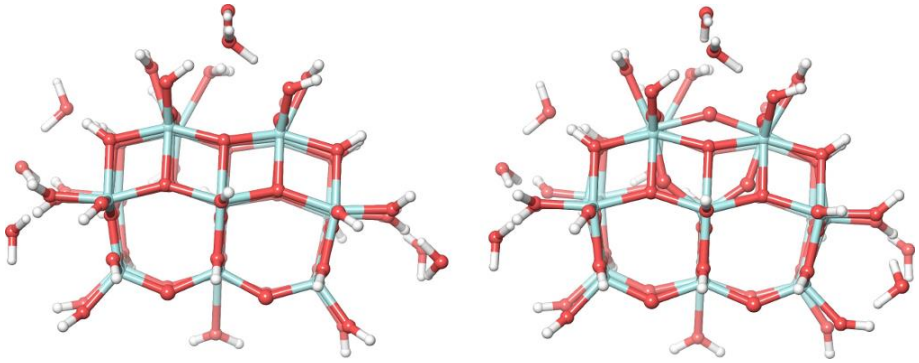

Figure 11 - Solvent-optimized neutral (left) and cationic (right) versions of the medium nanoparticle. Surface reconstruction can be seen in the cationic version.

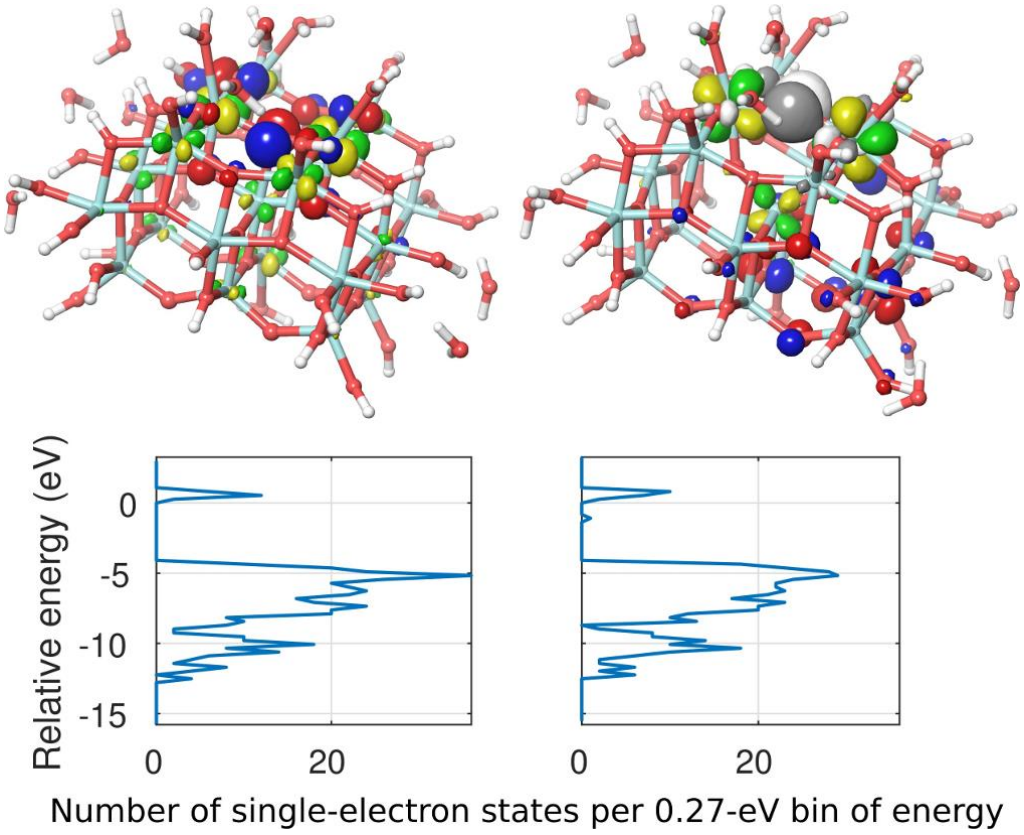

Figure 12 - Orbitals and densities of state of the clusters shown. (Top) Orbitals overlaid on the optimized geometries of the neutral (left) and cationic (right) versions of the medium nanoparticle. The HOMOs are colored blue/red and consist of primarily O2p atomic orbitals, the LUMOs are colored green/yellow and consist of primarily Ti_{3d} atomic orbitals, and the hole, which is centered on the topmost, reconstructing O atom, is colored white/gray and consists of primarily O_{2p} atomic orbitals. The neutral orbitals are two-particle and the cationic orbitals are one-particle. (Bottom) Corresponding plots of densities of state showing the valence band, the

band gap, and the 20 lowest-energy virtual spin orbitals that are outputted in the DFT calculations. The orbital energy of the hole in the cationic version is seen as the single state within the HOMO/LUMO gap.

The location of the beta HOMO (O_{2p}) in the neutral version of this nanoparticle is primarily the same as that of the hole in the cationic version, though the latter is even more localized. As expected, upon kicking an electron off the neutral version, giving the nanoparticle a $+1e$ charge, the beta LUMO initially has nearly the same energy as the beta HOMO in the neutral version and is located at nearly the same place. As the cationic optimization proceeds (and as surface reconstruction occurs), the beta LUMO, which is the hole orbital, increases from the HOMO energy to its final energy well within the band gap.

Fig. 13 and Tables 9 and 10 describe how the charges and bond lengths in the optimized cationic version of the nanoparticle change relative to those in the neutral version. The left graphic of subfigure (b) shows that the reconstructing O atom becomes significantly more positively charged (dark blue) and the center Ti atom significantly more negatively charged (dark red) as the donor-acceptor bond between them ("surface ring middle bond") breaks. Simultaneously, the other two O atoms and two Ti atoms that complete the six-atom "surface ring" become more positively and more negatively charged, respectively, though not to as large a degree. In addition, two Ti atoms (the "close" and "far" Ti atoms) become more negatively charged as the bonds they have with the two lower pinching-inward O atoms of the surface ring are stretched significantly, as shown by the blue "close bond" and the lack of a drawn "far bond" at all in subfigure (b). The total change in charge on these eight atoms is nearly zero ($0.02e$) even though five become more negatively charged and only three more positively charged, a testament to how much more positively charged the reconstructing O becomes due to the presence of the hole ($0.26e$) due exclusively to the hole and not including the positive contribution due to the

breaking of the surface ring middle bond. Throughout our studies we find that excess positive and negative charge, when not clearly associated with a particular orbital (such as the hole), tends to accumulate on bulk Ti atoms instead of bulk O atoms. Indeed, the 16 "uninvolved" Ti atoms in the medium nanoparticle system carry much of the +1*e* additional charge (0.56*e*), for an average increase of 0.03*e* on each atom, seen by the overall blue color of the remaining 16 large circles in the left graphic of subfigure (b).

Charges (e; cutoff = 0.037)			
Atom Name	**Neutral (a)**	**Cationic (b)**	**Notes**
Surface Ring O 1	-0.90	-0.53	Reconstructing O
Surface Ring O 2	-0.89	-0.81	Bottom DA O – surf.
Surface Ring O 3	-0.87	-0.80	
Surface Ring Ti 1	1.58	1.54	Surface Ti – surf.
Surface Ring Ti 2	2.12	1.88	Center Ti
Surface Ring Ti 3	1.62	1.57	
Close Ti	1.65	1.54	
Far Ti	1.59	1.51	
Avg. Uninvolved Ti	1.51	1.54	There are 16 of these

Table 9: Significantly changing charges of interest upon cationization and subsequent optimization of the medium nanoparticle. The corresponding plot of the changes in charge of all the atoms is shown in Fig. 5, to the subfigures which the letters identify in the column headers. DA means donor-acceptor.

Bond lengths (Å; cutoff = 0.079)			
Atom Name	**Neutral (a)**	**Cationic (b)**	**Notes**
Surface ring bond 1	1.94	2.06	
Surface ring bond 2	1.93	1.81	
Surface ring bond 4	1.93	1.82	
Surface ring bond 6	1.90	2.03	
Surface ring middle bond	2.11	3.45	

Close bond	2.16	2.78	
Far bond	2.24	2.95	

Table 10: Significantly changing bonds of interest upon cationization and subsequent optimization of the medium nanoparticle. The corresponding plot of the changes in bond lengths of all the bonds is shown in Fig. 5, to the subfigures which the letters identify in the column headers.

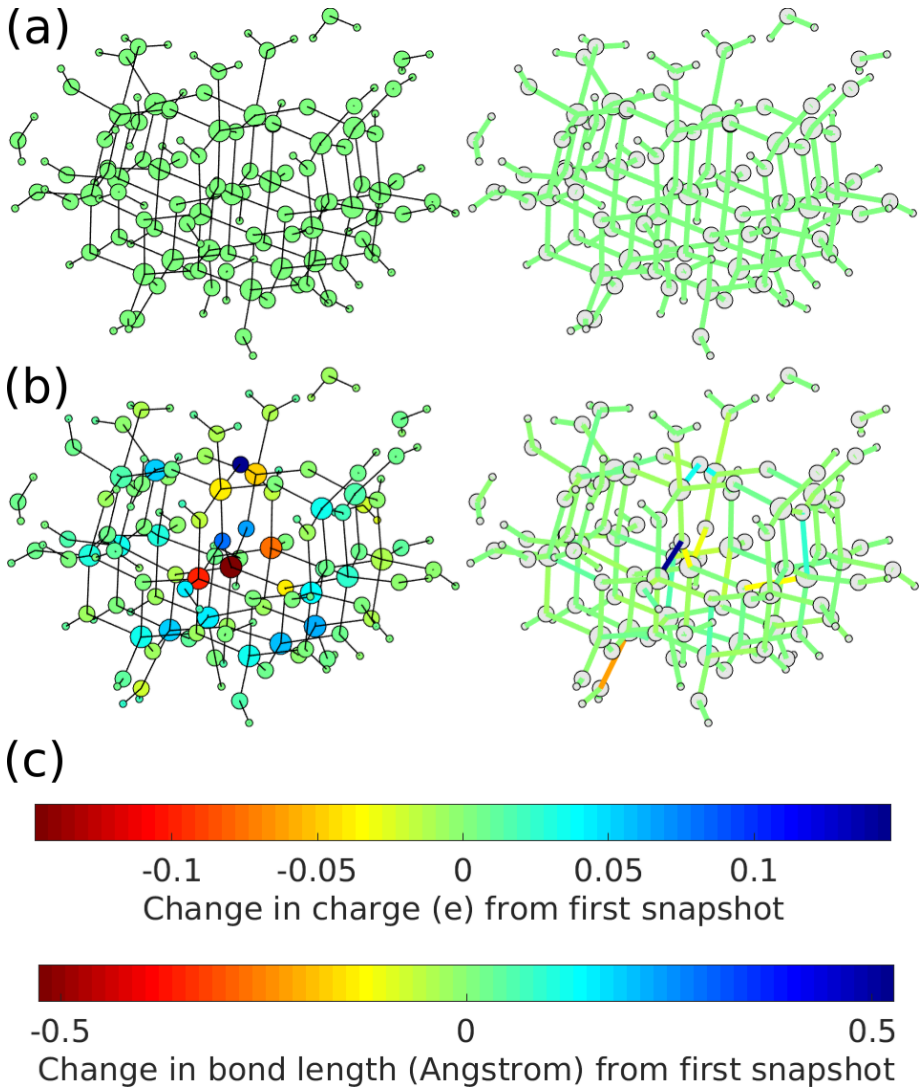

Figure 13 - Plot of how the charges (left) and bond lengths (right) change between the optimized (a) neutral version of the medium nanoparticle and the (b) cationic version. The nanoparticles in this figure are rotated roughly 90° about the $[001]$ direction from the orientations in other figures to better showcase the changing bonds. The numerical values of the important, significantly changing charges and bond lengths are listed in Tables 15 and 16, respectively. (c) Colorbars describing the change in charge (top) and bond length (bottom) of the other subfigures.

A.2.2 Large Nanoparticle

Geometry and electronic properties calculations were completed for both a neutral and a cationic large nanoparticle passivated with waters. The results of the neutral and cationic large nanoparticles largely align with those found for the medium nanoparticles (with the exception of the lack of surface reconstruction in the cationic nanoparticle that was observed in the medium cationic nanoparticle, discussed below). As in the medium nanoparticles, many of the surface-adsorbed, donor-accept-bonded water ligands readily disassociated from the (001) surface. We reiterate that in solvent water, substantially less than 100% coverage of the (001) surface is reasonable due to the molecular nature of their association to the (001) surface; adsorption on the (101) surface, conversely, is dissociative and thus complete.

The results (Table 11) from these large nanoparticle jobs reveal a bandgap of 4.04 eV in the neutral system and of 4.15 eV in the cationic system, with the hole 1.42 eV below the LUMO and 2.73 eV above the HOMO for the cationic nanoparticle. The band gap for the large nanoparticle system is smaller than that of the medium by about 0.5 – 0.6 eV for both charge states: this trend was expected again due to finite-size effect. Interesting to note is that, going from the medium to large nanoparticle, the decrease in band gap is due mostly to the valence band edge increasing in energy relative to the hole and conduction band edge. A Mulliken population analysis shows reveals the hole in the large cationic nanoparticle to reside on a surface O_{2c} atom, with the charge of the atom increasing from $-0.78e$ in the neutral large nanoparticle to $-0.54e$ in its cationic counterpart, an increase of $0.25e$. This is in contrast to an average charge on the other (001) surface O_{2c} atoms of $-0.77e$ for both the neutral and cationic clusters, and an average charge on the O_{3c} atoms in the layer beneath the (001) surface where the

hole resides of $-0.91e$ in both nanoparticles. No difference in charge on these oxygen atoms between the neutral and cationic nanoparticles exceeded $-0.01e$, except of course for the O_{2c} surface oxygen where the hole localized.

Energy (eV)		
	Medium Nanoparticle	Large Nanoparticle
Neutral nanoparticle band gap	4.62	4.04
Cationic nanoparticle band gap	4.58	4.15
Hole energy (above HOMO)	3.12	2.73
Hole energy (below LUMO)	1.46	1.42

Table 11 – Band gaps and hole energies for medium and large nanoparticle systems. Values for medium nanoparticle were taken from the "surface" cases. Note that hole energies only apply to cationic systems.

Although the results between the medium and large nanoparticle optimizations and electronic properties largely align, they are partially at odds with what we found in some versions of the medium cationic nanoparticle where a surface reconstruction occurred. Instead, interesting (if not more modest) local behavior at the top (001) surface of the nanoparticle is observed. In the neutral large nanoparticle, the bond lengths of same-type bonds are almost identical: the bonds along the surface between undercoordinated Ti atoms and bridging O atoms is, on average, between 1.81Å and 1.88Å. Although those on the edge are skewed a bit to be as high as 1.91Å or as low as 1.79Å, they occur in pairs to offset each other such that, in all cases, the sum of the two bonds coming from a bridging O (in a sense, the length of the entire oxygen bridge) is between 3.60Å and 3.67Å. For the large cationic nanoparticle, the same is true except for one important difference. For one bridging oxygen atom, the bond lengths on either side of the surface Ti atom are 2.03Å and 2.06Å, respectively. Together, these create a oxygen bridge length of 4.09Å, which is significantly larger than any other oxygen bridge length in either the

neutral or cationic system. Manual inspection reveals the two Ti atoms on either side of the bridging oxygen to be lengthening directly outward, parallel to the bonds. Additionally, visualization of the frontier orbitals of these systems show that, in the cationic case, the beta LUMO (corresponding to the newly created hole) localizes on this bridging oxygen atom. This makes sense, as a hole localized on this atom should weaken the bonds it makes, as it reduces the electron density available to that atom to make bonds with. So, while no reconstruction happens surrounding the bridging O atom where the hole is localized in the large cationic nanoparticle case as it does in some instances of medium cationic nanoparticle case, more modest spatial movements occur as a result of hole creation and localization that are in line with the rest of the results obtained from the medium nanoparticles. We suspect the reconstruction that occurs in some of the medium cationic nanoparticle cases is an artifact of the unrealistically small size of the system or the freezing of the Ti atoms necessary to have a well-defined reaction coordinate, and that it had little impact on the total system energies obtained.

A.3 Detailed Pulling Experiments Results

A.3.1 Medium Nanoparticle

Although we focused on the systems where we pulled the H^+ participating in the PCET from a water molecule squarely on the (001) surface of the medium nanoparticle (“surface” case) in the main body of this thesis, particularly the cationic system, we also performed these pulling experiments on a water ligand located at the edge of the (001) surface (“edge” case), constituting four pulling experiments on the medium nanoparticle: the neutral/surface case, the cationic/surface case, the neutral/edge case, and the cationic/edge case. We focus on the

"surface" cases in the main body of this thesis mainly because it is the analogue case to our bigger, more instructive large nanoparticle pulling experiment and because the difference between the edge and surface cases on the nanoparticle are relatively minor, if not still interesting in their own right. Here we compare them with the "edge" cases.

Snapshots (b) in Figs. 7, 14, 15, and 16 show that as the solvent H_2O is placed near the adsorbed H_2O, the charge on the transferring H^+ increases on average from $0.46e$ to $0.49e$ in the four pulling experiments; that on the adsorbate's O atom decreases on average from $-0.73e$ to $-0.79e$ in the four cases; and that on the Ti atom on the surface decreases from $1.53e$ to $1.51e$ in the cationic/surface case and increases from $1.52e$ to $1.57e$, $1.58e$ to $1.60e$, and $1.47e$ to $1.56e$ in the cationic/edge, neutral/surface, and neutral/edge cases, respectively.

The bond between the transferring H^+ and the adsorbate O lengthens on average from 0.98Å to 1.01Å in the four cases and that between the adsorbate O and the surface Ti ("top donor-acceptor bond") shortens on average from 2.24Å to 2.16Å in the surface cases and from 2.39Å to 2.23Å in the edge cases.

These results provide further evidence of a potential mechanism for the initial separation of charge required for the PCET: as the negatively charged O atom of the solvent H_2O pushes negative charge from the transferring H^+ (making it more positive) to the adsorbate O (making it more negative), it simultaneously pulls on the positively charged transferring H^+ itself, lengthening the bond between the H^+ and the adsorbate O.

We note that since the distance and location between the adsorbed H_2O and the nearby H_2O is arbitrary in snapshots (b) (solvent molecule arbitrarily close to the nanoparticle), it is difficult to compare between the specific cases (cationic vs. neutral, surface vs. edge) for this snapshot. However, since in all four pulling experiments snapshots (c) through (e) depict the

system in well-defined states — just before the H^+ transfer, just after the H^+ transfer, and with the H_3O^+ effectively pulled infinitely far away, respectively — it is more valid to make comparisons between specific cases for these snapshots, as we do now.

Snapshots (c) show that as the transferring H^+ is pulled further without yet transferring to the solvent H_2O, there is a fundamental difference between the surface and edge cases: in the latter, the bond between the Ti atom on the surface and the O atom beneath it ("bottom donor-acceptor bond") breaks, as if the force of the pulling on the H^+ is exerted through the attached adsorbate O and surface Ti and literally pulls the bottom donor-acceptor bond apart. This greatly affects the charges and bond lengths in the system, making doing the pulling experiment for edge cases more cumbersome.

Regardless, the charge on the adsorbate's non-transferring H atom decreases on average from $0.46e$ to $0.45e$ in the surface cases and increases on average from $0.46e$ to $0.48e$ in the edge cases; that on the transferring H^+ decreases on average from $0.49e$ to $0.47e$ in the surface cases and increases on average from $0.48e$ to $0.49e$ in the edge cases; that on the adsorbate O increases on average from $-0.79e$ to $-0.77e$ in the surface cases and decreases on average from $-0.78e$ to $-0.80e$ in the edge cases; that on the surface Ti remains at $1.51e$ in the cationic/surface case, decreases from $1.60e$ to $1.57e$ in the neutral/surface case, and decreases on average from $1.57e$ to $1.48e$ in the edge cases; and that on the O atom beneath the surface Ti atom ("bottom donor-acceptor O") remains at $-0.82e$ in the cationic/surface case and at $-0.90e$ in the neutral/surface case and increases on average from $-0.93e$ to $-0.78e$ in the edge cases. The top donor-acceptor bond lengthens on average from 2.16Å to 2.25Å in the surface cases and shortens on average from 2.23Å to 2.13Å in the edge cases.

Snapshots (d) show that just after the H^+ transfers to the nearby H_2O, in the surface cases the surface Ti moves upward toward the adsorbate, simultaneously shortening the top donor-acceptor bond and lengthening the bottom donor-acceptor bond. We posit that the Ti moves upward — rather than the entire adsorbate moving downward — because even though the H^+ has moved away, allowing the positively charged Ti to be attracted to the negative charge the H^+ left behind on the remaining H and adsorbate O, the H^+ is still near the negatively charged adsorbate O and the left-behind negative charge and therefore holds the adsorbate in place through electrostatic attraction. Though near-subsequent snapshots are not shown, as the H_3O^+ is pulled farther away from the configuration in (d), the surface Ti — and therefore the entire adsorbate — settles downward back into the nanoparticle, likely because the positively charged H_3O^+ attracts the adsorbate O and the negative charge left behind by the H^+ less and less. Thus, the charges and bond lengths on the system gradually equilibrate to their final values of snapshots (e). In contrast, as the H^+ transfer occurs in the edge cases, the bottom donor-acceptor bond immediately snaps back together and the charges and bond lengths on the system nearly immediately acquire their final values of snapshots (e).

In snapshots (d), the charge on the adsorbate's remaining H atom decreases on average from $0.45e$ to $0.40e$ in the surface cases and from $0.48e$ to $0.42e$ in the edge cases; that on the adsorbate O decreases on average from $-0.77e$ to $-0.80e$ in the surface cases and increases on average from $-0.80e$ to $-0.75e$ in the edge cases; that on the surface Ti decreases from $1.51e$ to $1.42e$, $1.49e$ to $1.48e$, $1.57e$ to $1.52e$, and $1.47e$ to $1.42e$ in the cationic/surface, cationic/edge, neutral/surface, and neutral/edge cases, respectively; that on the bottom donor-acceptor O increases from $-0.82e$ to $-0.77e$ in the cationic/surface case and from $-0.90e$ to $-0.88e$ in the neutral/surface case and decreases on average from $-0.78e$ to $-0.86e$ in the edge cases;

that on the H_3O^+ increases on average from 0.57*e* to 0.88*e* in the surface cases and from 0.59*e* to 1.01*e* in the edge cases; and that on the adsorbate+H_3O^+ system increases on average from 0.25*e* to 0.49*e* in the surface cases and from 0.28*e* to 0.68*e* in the edge cases.

The top donor-acceptor bond shortens from 2.24Å to 2.00Å in the cationic/surface case, from 2.26Å to 2.10Å in the neutral/surface case, and on average from 2.13Å to 1.89Å in the edge cases and the bottom donor-acceptor bond lengthens on average from 1.92Å to 2.17Å in the surface cases and goes from unbonded to an average of 2.41Å in the edge cases.

Snapshots (e) show that after the H_3O^+ is pulled far away from the nanoparticle, overall, in all cases the top donor-acceptor bond shortens, the bottom donor-acceptor bond lengthens, and negative charge has flowed from the adsorbate into the nanoparticle. In the surface cases the largest concentration of this negative charge is on the surface Ti atom, and in the edge cases this higher concentration of negative charge is more or less distributed amongst the three Ti atoms (which includes the surface Ti atom) making up the six-atom "edge ring" whose inner bond is the bottom donor-acceptor bond.

The charge on the adsorbate O increases on average from $-0.80e$ to $-0.75e$ in the surface cases and decreases on average from $-0.75e$ to $-0.76e$ in the edge cases; that on the surface Ti decreases from 1.42*e* to 1.40*e*, increases from 1.48*e* to 1.49*e*, decreases from 1.52*e* to 1.50*e*, and decreases from 1.42*e* to 1.41*e* in the cationic/surface, cationic/edge, neutral/surface, and neutral/edge cases, respectively; that on the bottom donor-acceptor O remains at $-0.77e$ in the cationic/surface case, increases from $-0.88e$ to $-0.87e$ in the neutral/surface case, and decreases on average from $-0.86e$ to $-0.88e$ in the edge cases; that on the H_3O^+ becomes exactly 1.00*e* in all four cases; and that on the adsorbate + H_3O^+ system becomes on average 0.67*e* in all four cases. The top donor-acceptor bond shortens from 2.00Å to 1.88Å in the

cationic/surface case, from 2.10Å to 1.89Å in the neutral/surface case, and remains at an average of 1.89Å in the edge cases and the bottom donor-acceptor bond shortens from 2.19Å to 2.09Å, shortens from 2.38Å to 2.25Å, lengthens from 2.16Å to 2.18Å, and shortens from 2.45Å to 2.28Å in the cationic/surface, cationic/edge, neutral/surface, and neutral/edge cases, respectively.

Comparing briefly the surface case to the edge case for each of the cationic and neutral pulling experiments on the medium nanoparticle, we see that based on thermodynamics alone the surface cases require less energy than the edge cases (by 0.19 eV for the cationic nanoparticle and 0.18 eV for the neutral nanoparticle) and that when kinetic contributions are taken into account, the same conclusions hold). While one need not study the kinetics of the PCET to come to the conclusion that it is more likely to occur at a surface adsorbate than at an edge adsorbate by chance, such a study as this affords a physical explanation for this, as we provided in Section 4.3.2 when we discussed the electron transfer that occurs during this process. We note that this conclusion is in contrast to studies [4] suggesting that the OER occurs more readily at edges (and steps, which have similar structures as edges) than on surfaces.

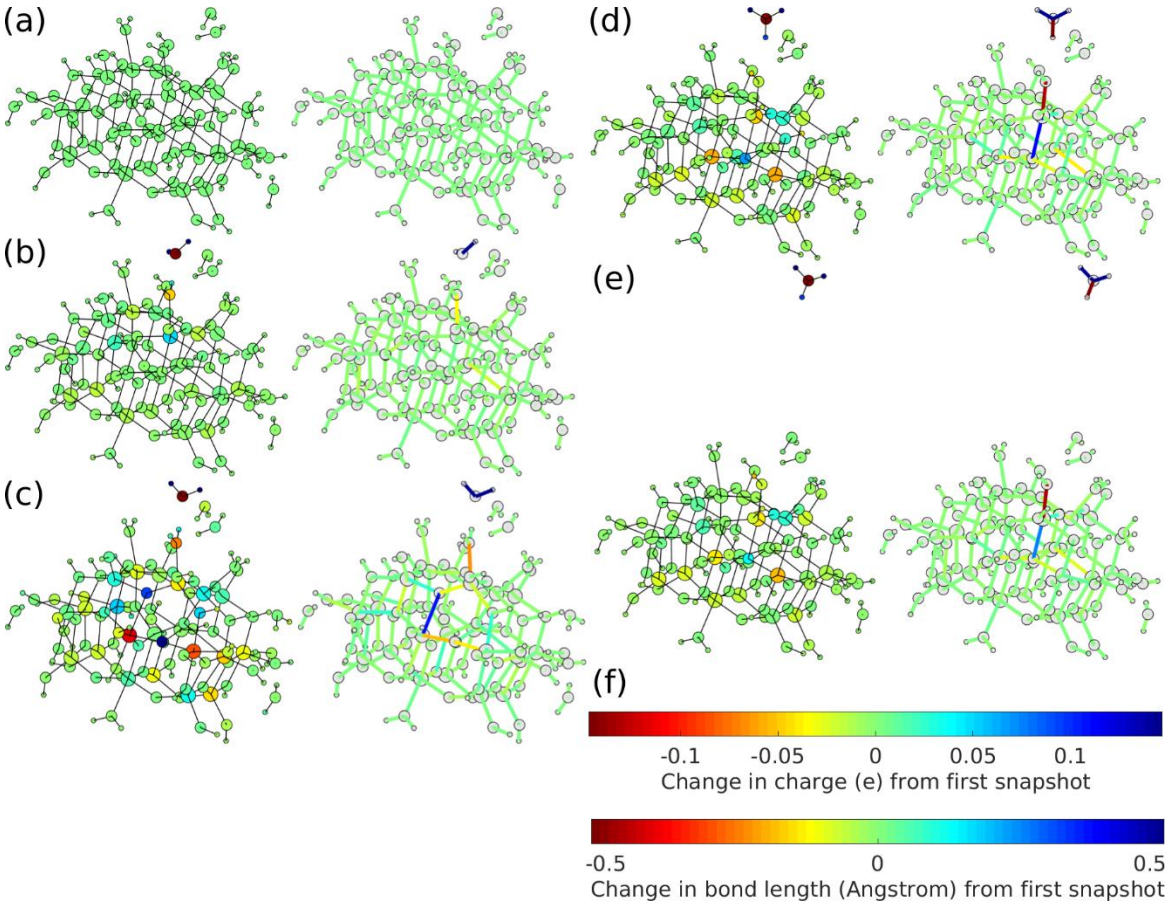

Figure 14 – Changes in charge (left of each subfigure) and bond length (right of each subfigure) for selected snapshots of the pulling experiment performed on the medium, cationic nanoparticle from an “edge” water adsorbate relative to the properties for (a) the cationic nanoparticle with no nearby explicit water added. (b) First datapoint of the pulling experiment; 7.03 Å. (c) Datapoint 3; 7.63 Å. (d) Datapoint 4; 7.73 Å. (e) Datapoint 17; 16.03 Å. (f) Colorbars describing the change in charge (top) and bond length (bottom) of the other subfigures. The numerical values of the important, significantly changing charges and bond lengths are listed in Tables 12 and 13.

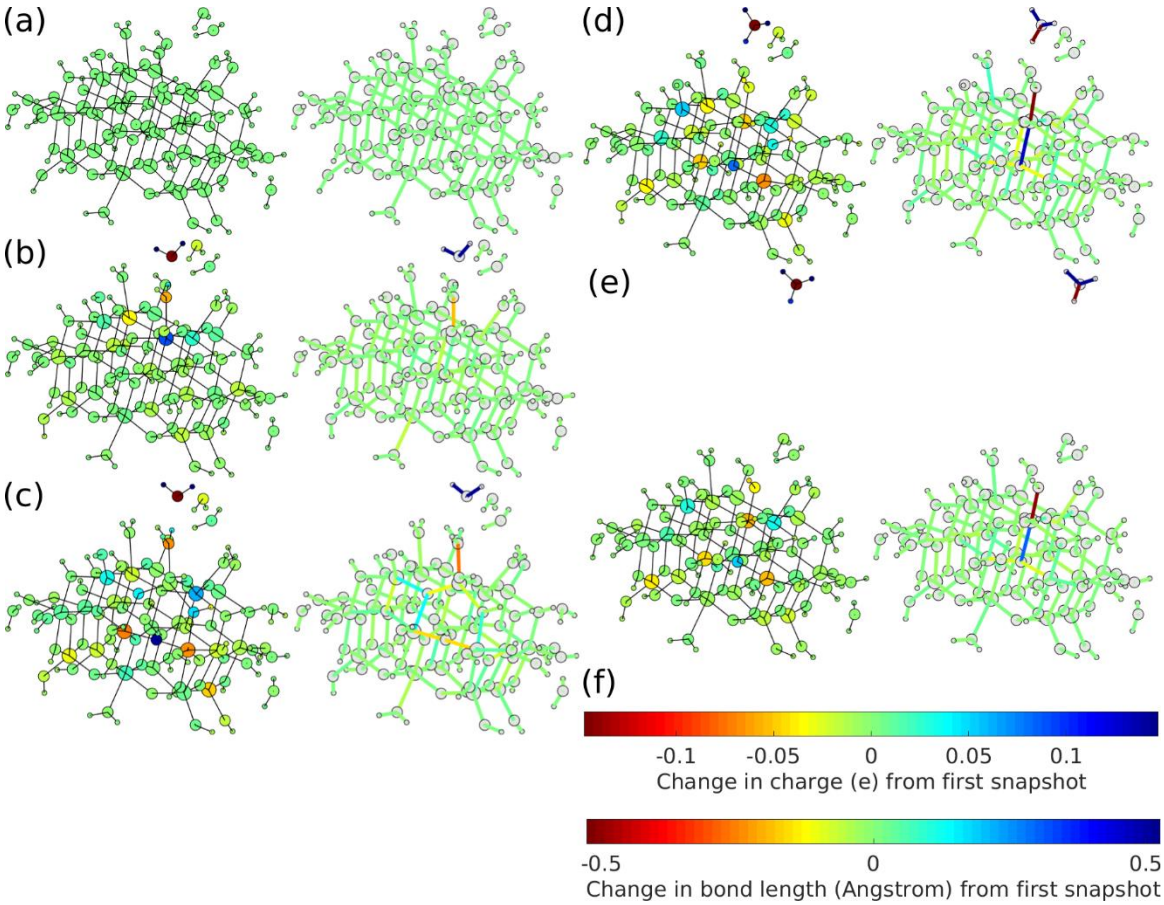

Figure 15 – Changes in charge (left of each subfigure) and bond length (right of each subfigure) for selected snapshots of the pulling experiment performed on the medium, neutral nanoparticle from an “edge” water adsorbate relative to the properties for (a) the cationic nanoparticle with no nearby explicit water added. (b) First datapoint of the pulling experiment; 7.03 Å. (c) Datapoint 3; 7.63 Å. (d) Datapoint 4; 7.73 Å. (e) Datapoint 17; 16.03 Å. (f) Colorbars describing the change in charge (top) and bond length (bottom) of the other subfigures. The numerical values of the important, significantly changing charges and bond lengths are listed in Tables 14 and 15.

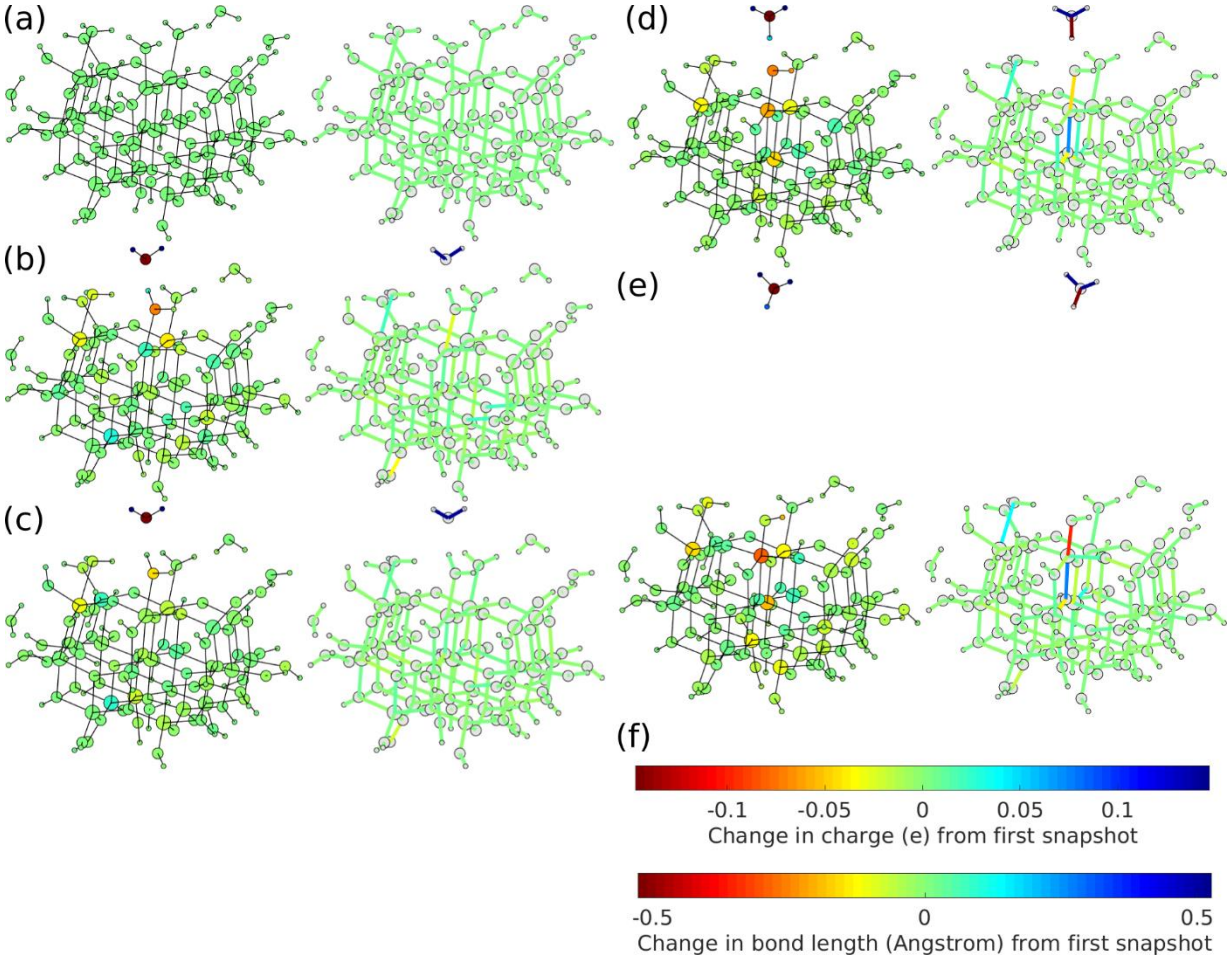

Figure 16 – Changes in charge (left of each subfigure) and bond length (right of each subfigure) for selected snapshots of the pulling experiment performed on the medium, neutral nanoparticle from a "surface" water adsorbate relative to the properties for (a) the cationic nanoparticle with no nearby explicit water added. (b) First datapoint of the pulling experiment; 7.03 Å. (c) Datapoint 3; 7.63 Å. (d) Datapoint 4; 7.73 Å. (e) Datapoint 17; 16.03 Å. (f) Colorbars describing the change in charge (top) and bond length (bottom) of the other subfigures. The numerical values of the important, significantly changing charges and bond lengths are listed in Tables 16 and 17.

Charges (e; cutoff=0.037*)*						
Atom name	**(a)**	**(b)**	**(c)**	**(d)**	**(e)**	**Notes**
Close Ti	1.55	1.55	1.50	1.55	1.54	
Edge ads. H 1	0.46	0.48	0.49	0.55	0.55	Transferring H − edge
Edge ads. H 2	0.46	0.46	0.48	0.42	0.41	Other adsorbate H – edge
Edge ads. O	−0.73	−0.78	−0.80	−0.74	−0.75	Adsorbate

						O – edge
Edge ring O 1	−0.92	−0.92	−0.83	−0.92	−0.92	
Edge ring O 2	−0.93	−0.93	−0.78	−0.86	−0.89	Bottom DA O – edge
Edge Ring O 3	−0.88	−0.87	−0.83	−0.85	−0.87	
Edge Ring Ti 1	1.52	1.57	1.49	1.48	1.49	Surface Ti − edge
Edge Ring Ti 2	1.63	1.63	1.51	1.57	1.59	
Edge ring Ti 3	1.59	1.59	1.51	1.53	1.54	
Avg. uninvolved Ti	1.59	1.55	1.55	1.55	1.55	There are 17 of these

Table 12 – Significantly changing charges of interest during the cationic/edge medium nanoparticle pulling experiment. The corresponding plot of the changes in charge is shown in Fig. 16, to the subfigures to which the letter identifiers in the column headers refer.

Bond Lengths (Å; cutoff=0.079*)*						
Bond name	**(a)**	**(b)**	**(c)**	**(d)**	**(e)**	**Notes**
Close bond	2.76	2.69	2.81	2.62	2.68	
Edge Ti − O	2.37	2.24	2.13	1.89	1.89	Top DA – edge
Edge ring bond 1	1.91	1.89	1.79	1.88	1.90	
Edge ring bond 2	2.02	2.04	2.41	2.06	2.05	
Edge ring bond 3	2.00	1.98	1.80	1.88	1.91	
Edge ring bond 4	1.98	1.97	1.84	1.88	1.90	
Edge ring bond 5	1.97	1.98	2.06	2.02	2.00	
Edge ring middle bond	1.97	2.00	3.23	2.38	2.25	Bottom DA – edge

Table 13 – Significantly changing bond lengths of interest during the cationic/edge medium nanoparticle pulling experiment. The corresponding plot of the changes in bond lengths is shown in Fig. 16, to the subfigures to which the letter identifiers in the column headers refer.

Charges (e; cutoff=0.037*)*						
Atom name	**(a)**	**(b)**	**(c)**	**(d)**	**(e)**	**Notes**
Surface ring Ti 1	1.58	1.60	1.64	1.61	1.61	Surface Ti – surf.
Edge ads. H 1	0.45	0.48	0.49	0.55	0.55	Transferring H − edge
Edge ads. H 2	0.46	0.45	0.48	0.43	0.42	Other adsorbate H – edge
Edge ads. O	−0.73	−0.78	−0.79	−0.75	−0.76	Adsorbate O – edge
Edge ring O 1	−0.93	−0.93	−0.89	−0.93	−0.93	
Edge ring O 2	−0.93	−0.93	−0.79	−0.85	−0.88	Bottom DA O – edge
Edge Ring O 3	−0.87	−0.87	−0.82	−0.84	−0.87	
Edge Ring Ti 1	1.47	1.56	1.47	1.42	1.41	Surface Ti − edge
Edge Ring Ti 2	1.59	1.60	1.52	1.55	1.55	
Edge Ring Ti 3	1.57	1.56	1.50	1.50	1.51	
Avg. uninvolved Ti	1.59	1.55	1.55	1.55	1.55	There are 17 of these

Table 14 – Significantly changing charges of interest during the neutral/edge medium nanoparticle pulling experiment. The corresponding plot of the changes in charge is shown in Fig. 17, to the subfigures to which the letter identifiers in the column headers refer.

*Bond Lengths (*Å*; cutoff*=0.079*)*						
Bond name	**(a)**	**(b)**	**(c)**	**(d)**	**(e)**	**Notes**
Surface ring middle bond	2.11	2.06	2.07	2.01	2.05	
Edge Ti − O	2.41	2.21	2.13	1.88	1.89	Top DA – edge
Edge ring bond 1	1.92	1.91	1.82	1.88	1.91	
Edge ring bond 2	1.99	2.01	2.14	2.04	2.03	
Edge ring bond 3	1.98	1.97	1.81	1.87	1.89	

Edge ring bond 4	1.99	1.97	2.05	2.02	2.01	
Edge ring bond 5	1.96	1.97	2.05	2.02	2.01	
Edge ring middle bond	1.97	2.01	3.10	2.45	2.28	Bottom DA – edge

Table 15 – Significantly changing bond lengths of interest during the neutral/edge medium nanoparticle pulling experiment. The corresponding plot of the changes in bond lengths is shown in Fig. 17, to the subfigures to which the letter identifiers in the column headers refer.

Charges (e; cutoff=0.037*)*						
Atom name	**(a)**	**(b)**	**(c)**	**(d)**	**(e)**	**Notes**
Surface ads. H 1	0.46	0.49	0.47	0.51	0.55	Transferring H – surf.
Surface ads. H 2	0.46	0.46	0.45	0.40	0.41	Other adsorbate H – surf.
Surface ads. O	−0.73	−0.80	−0.77	−0.80	−0.74	Adsorbate O – surf.
Surface ring Ti 1	1.58	1.60	1.57	1.52	1.50	Surface Ti – surf.
Surface ring Ti 2	2.12	2.10	2.11	2.07	2.06	Center Ti
Surface ring Ti 3	1.62	1.58	1.60	1.59	1.58	
Edge ring Ti 1	1.47	1.44	1.44	1.44	1.43	Surface Ti – edge
Average uninvolved Ti	1.52	1.53	1.53	1.52	1.52	There are 17 of these

Table 16 – Significantly changing charges of interest during the neutral/surface medium nanoparticle pulling experiment. The corresponding plot of the changes in charge is shown in Fig. 18, to the subfigures to which the letter identifiers in the column headers refer.

*Bond Lengths (*Å*; cutoff*=0.079*)*						
Bond name	**(a)**	**(b)**	**(c)**	**(d)**	**(e)**	**Notes**
Surface Ti – O	2.26	2.17	2.26	2.10	1.89	Top DA – surf.

Surface ring bond 2	1.91	1.94	1.94	2.16	2.18	Bottom DA – surf.
Surface ring bond 3	1.93	1.89	1.89	1.84	1.83	
Surface ring bond 4	1.93	1.97	1.96	1.98	2.03	
Close bond	2.16	2.13	2.12	2.03	2.02	
Edge Ti – O	2.41	2.48	2.45	2.50	2.56	Top DA – edge

Table 17 – Significantly changing bond lengths of interest during the neutral/surface medium nanoparticle pulling experiment. The corresponding plot of the changes in bond lengths is shown in Fig. 18, to the subfigures to which the letter identifiers in the column headers refer.